2013

Liquid sorption properties and structural changes of metal-organic frameworks of cobalt nitrate and 4,4'-bipyridine

Kathryn Mauger-Sonnek
University of Northern Iowa

LIQUID SORPTION PROPERTIES AND STRUCTURAL CHANGES OF METAL-ORGANIC FRAMEWORKS OF COBALT NITRATE AND 4,4′-BIPYRIDINE

An Abstract of a Thesis

Submitted

in Partial Fulfillment

of the Requirements for the Degree

Master of Science

Kathryn Mauger-Sonnek

University of Northern Iowa

August 2013

ABSTRACT

Metal-organic frameworks consist of metal ions connected by organic ligands. When the metal ions and organic ligands link together in the right geometry, polymeric and infinite 1D chains or 2D and 3D networks are formed. Porous metal-organic frameworks were synthesized from the organic ligand 4,4′-bipyridine (bpy) and cobalt(II) nitrate. The metal-organic frameworks synthesized in this study grew into both a previously known 2D bilayer structure, $[Co_2(bpy)_3(NO_3)_4]_n$, and a new, orange 1D chain structure, $[Co(bpy)NO_3)_2(H_2O)_2]_n$, within ethanol. It was found that the presence of water was the main factor of causing formation of the orange 1D chain crystals. Drying the orange 1D chain crystals in an oven removed the solvent from the pores and the aqua ligands, but the sample retained its crystallinity and the 1D chain structure. Both the red bilayer and purple 1D chain crystals lost their single crystallinity when resolvated with water vapor. However, when the bilayer was dried and re-exposed to ethanol vapor, it returned to its original, as synthesized structure. Sorption studies were conducted on the red bilayer crystals using gas chromatograph measurements. It was found that the pores were selective to the solvents *n*-hexane and ethanol, primarily due to liquid guest molecule size.

LIQUID SORPTION PROPERTIES AND STRUCTURAL CHANGES OF METAL-ORGANIC FRAMEWORKS OF COBALT NITRATE AND 4,4′-BIPYRIDINE

A Thesis

Submitted

in Partial Fulfillment

of the Requirements for the Degree

Master of Science

Kathryn Elizabeth Mauger-Sonnek

University of Northern Iowa

August 2013

This Study by: Kathryn Mauger-Sonnek

Entitled: Liquid Sorption Properties and Structural Changes of Metal-Organic Polymers of Cobalt Nitrate and 4,4′-Bipyridine

has been approved as meeting the thesis requirement for the

Degree of Master of Science

_____	_____
Date	Dr. Colin Weeks, Chair, Thesis Committee
_____	_____
Date	Dr. Laura Strauss, Thesis Committee Member
_____	_____
Date	Dr. Melisa Cherney, Thesis Committee Member
_____	_____
Date	Dr. Michael J. Licari, Dean, Graduate College

TABLE OF CONTENTS

PAGE

PAGE

PAGE

LIST OF TABLES

LIST OF FIGURES

FIGURE PAGE

FIGURE PAGE

FIGURE PAGE

FIGURE PAGE

CHAPTER 1

INTRODUCTION

Structure of Metal Organic Frameworks

Metal organic frameworks (MOFs) are formed when metal ions are linked together by bridging organic ligands into extended networks. The metal ions can have different coordination geometries as shown in Figure 1.1. Organic ligands can have multiple binding sites that are oriented so that they bind to different metal ions (Figure 1.2). The possible types of frameworks are endless due to the vast number of possible combinations of metal ions and organic linkers that can be used.

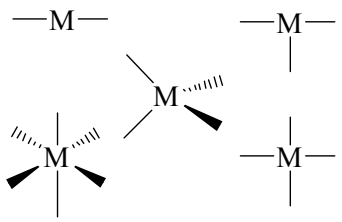

Figure 1.1 Examples of coordination geometries of ligands around a metal ion

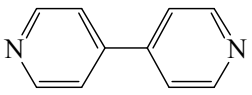

4,4′-bipyridine (bpy)

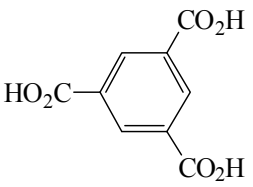

1,3,5-benzenetricarboxylic acid

Figure 1.2 Examples of organic bridging ligands used to form MOFs

Due to this wide variety of coordination geometries, many types of MOFs exist and form 1D, 2D, and 3D frameworks. These categories are based on how many dimensions the polymeric connectivity extends to in the structure. Examples of 1D framework topologies include the chain and ladder structure shown in Figure 1.3. Examples of 2D frameworks include the honeycomb and square grid as shown in Figure 1.4. A diagram of a 3D framework diamondoid is shown in Figure 1.5.

A

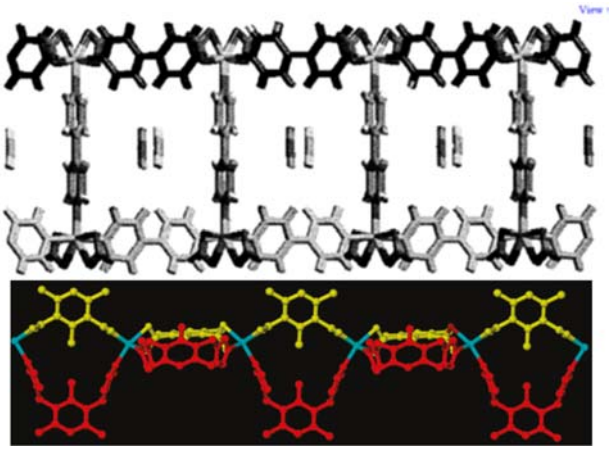

B

Figure 1.3 Example of 1D ladder (A)[1] and 1D chain (B)[2] MOFs

A

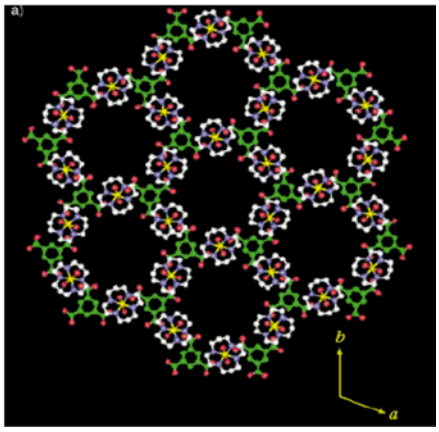

B

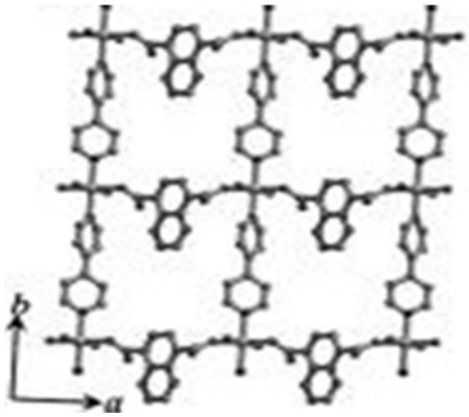

Figure 1.4 Example of 2D honeycomb (A)[3] and 2D square grid (B)[1]MOFs

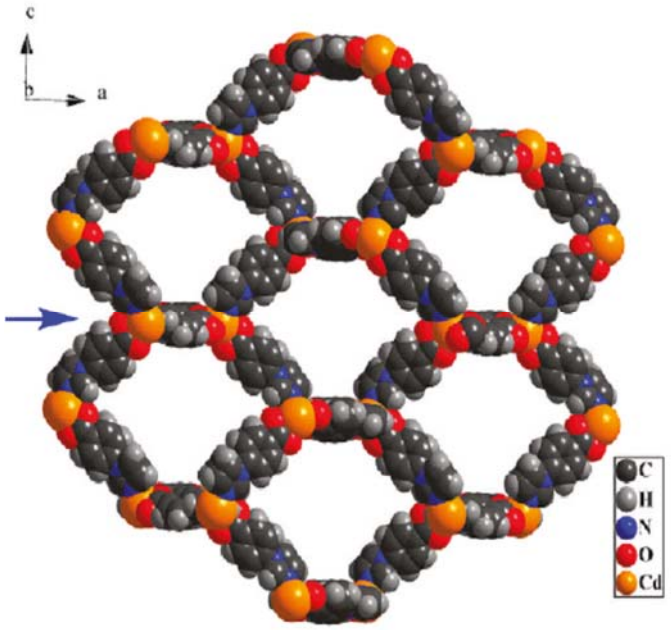

Figure 1.5 An example of a 3D diamondoid[4] MOF

Formation of MOFs

MOFs can form by the processes of solvothermal synthesis or by slow diffusion of the framework building blocks at room temperature. Solvothermal synthesis requires all framework components and solvent to be added to a teflon-lined bomb which is placed inside an oven.[5] The pressure vessel allows for a high solution temperature which causes dissolution of all framework building blocks.[6] As the solution is slowly cooled (usually over a period of 24-72 hours), crystal formation occurs.[6] Room temperature diffusion involves layering solutions of the ligand and metal ion on top of each other, usually in an organic solvent, within a vial or H-cell to allow for slow diffusion of the components to

form the crystalline structures. The layering of solutions is sometimes performed while the vials are in an ice bucket to slow down diffusion and mixing of layers.[7]

The advantage of using solvothermal synthesis is the production of crystals within a short period of a few days.[6] Since Teflon-lined bombs are utilized, this method is also very useful for dissolving components at high pH.[6] Room temperature diffusion is a somewhat tedious process as concentrations must be tuned to create an ideal rate of component diffusion. However, this can sometimes create a variety of frameworks within the same vial or H-cell as the metal ions and ligands have time to rearrange into different coordination complexes.[7]

Benefits of MOFs

Throughout the past twenty years, MOFs have been developed and their interesting properties demonstrated.[8] MOFs have been shown to have good thermal stability, and are often stable up to 400ºC. [5] They also have well-defined pore sizes and high surface area[5], making them ideal for liquid[8,9,10,11] and gas sorption. [6,12,13,14] It has been demonstrated that MOFs have magnetic,[15,16] luminescent,[10,17] and catalytic[18,19,20] properties as well.

Magnetism

MOFs have magnetic properties due to the partially filled *d* or *f* orbitals of the metal. MOFs constructed using the first row transition metals can either be high spin or low spin depending on the ligand field strength, allowing for the property of spin crossover. Spin crossover was found to be both temperature and solvent dependent in the porous framework of $[Fe_2(azpy)_4(NCS)_4]_n$ (azpy=azopyridine and NCS=thiocyanate) (Fig 1.6).[16]

When the ethanol solvent was removed from the pores, the framework no longer exhibited temperature dependent spin crossover. When the material was resolvated with ethanol, the temperature dependent spin crossover was restored.[16] Another framework, $[Co_3(cis\text{-}CHHC)(H_2O)_8]_n \cdot 5H_2O$ (CHHC=cis 1,2,3,4,5,6-cyclohexanehexacarboxylate), was found to have antiferromagnetic coupling between the metal ions.[15]

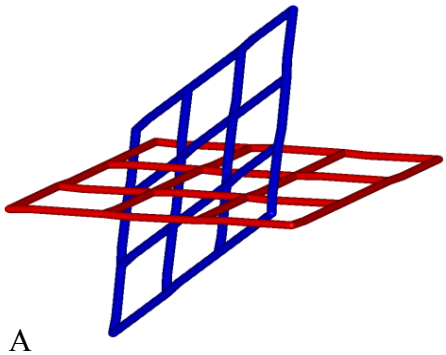

A

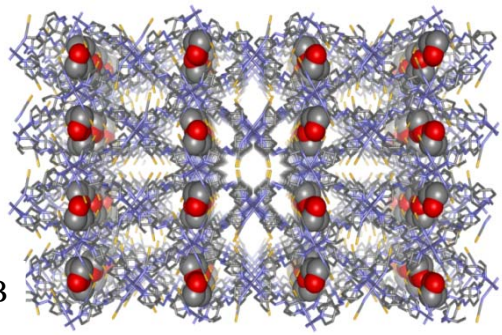

B

Figure 1.6 Schematic diagram of interpenetrating 2D grid structure (A) and molecular structure (B) of $[Fe_2(azpy)_4(NCS)_4]_n$ showing ethanol solvent molecules in the pores[16]

Luminescence

When exposed to specific solvents, MOFs can demonstrate luminescence, phosphorescence, and scintillation.[17] This happens due to hydrogen bonding interactions between the ligands and solvent anions causing a transformation in luminescence

intensity.[10] One example is the framework Tb(BTC) (BTC=benzene-1,3,5-tricarboxylate), which was found to have photoluminescent properties when sodium chloride mixed in methanol was introduced to the pores.[10] Interactions between the oxygen of the methanol (purple) and the chloride anions (green) are shown in Figure 1.7. The level of luminescence intensity varied when using different types of salt solutions as shown in Figure 1.8.[10]

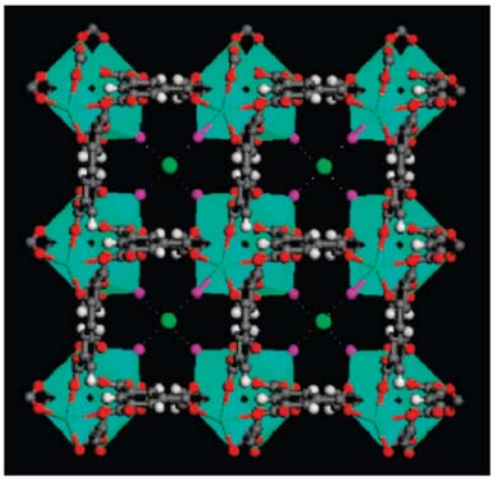

Figure 1.7 Tb(BTC) framework with hydrogen bonding between BTC ligands and anions in solvent[10]

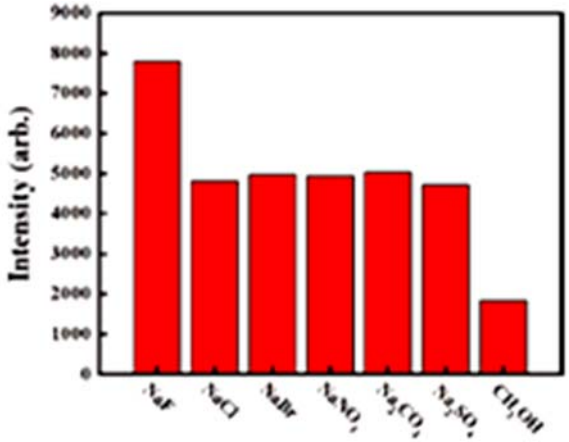

Figure 1.8 Intensity using different salt solutions[10]

Catalysis

MOFs offer great potential for uses as catalysts. The metal ion of some frameworks can act as a binding site for the substrate as shown in Fig 1.9. When designing these pores, it is important to both introduce unsaturated metal centers into the framework and create voids for selective catalysis. MOFs have been shown to catalyze many organic reactions. One particularly successful example involves an indium framework $[In(OH)_3(BDC)_{1.5}]_n$ (BDC=1,4-benzenedicarbozylate) that was active in the hydrogenation of nitroaromatics and oxidation of organic sulfides (Fig 1.10).[20] For this framework, a high yield of product was produced with high turnover frequencies of 489 and 385 min^{-1}. Within 6 hours, a 100% yield of hydrogenated product was obtained. Also, the framework was found to be reusable without reactivation four times.[20] Examples of frameworks that have been used as catalysts in the literature include $[Co(N,N'\text{-dimethylacetamide})_6]_3[(Co_4Cl)_3\text{-}(1,2,3\text{-benzetristetrazolate})_8(H_2O)_{12}]_2 \cdot 12H_2O$ that catalyzes the oxidation of cycloalkanes and benzyl compounds,[18] $[M(H_2O)_6(1,3,5\text{-}$

benzenetricarboxylate)$_2$] that catalyzes the oxidation phenols, and [M_2(1,10-phenanthroline)$_2$(H_2O)$_2$]$_2$ (where M= Ni(II), Cu(II), Zn(II) and Mn(II)) that catalyzes the oxidation of phenols.[19,20]

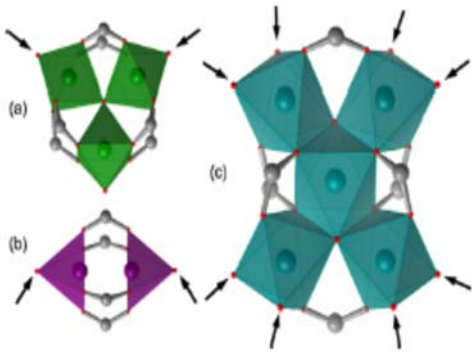

Figure 1.9 Diagram of metal ion sites of hypothetical MOFs that can act as points for interaction with a substrate[21]

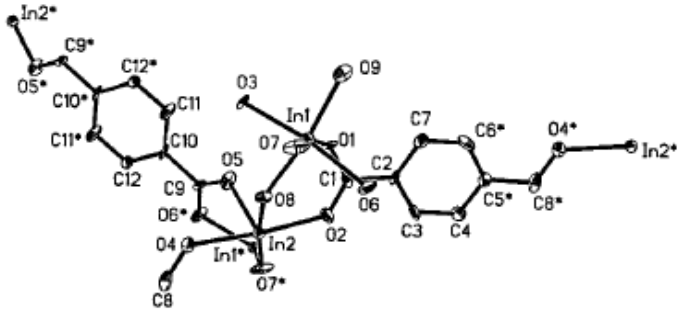

Figure 1.10 Structure of [In(OH)$_3$(BDC)$_{1.5}$]$_n$[20]

Liquid Sorption Properties

The ability to separate mixtures of organic compounds in the small pore volumes of MOFs could reduce the amount of eluents requires in chromatographic separation and reduce purification costs up to 60%.[8] Liquid sorption studies are also important for understanding other MOF properties. Liquid sorption behavior determines substrate entry into MOF catalysts and product escape and can be used to tune other properties such as magnetism and luminescence.[10,15] Often guest molecule sorption into the pores can change the shape and structure of a MOF as well (Figure 1.11).[6,14]

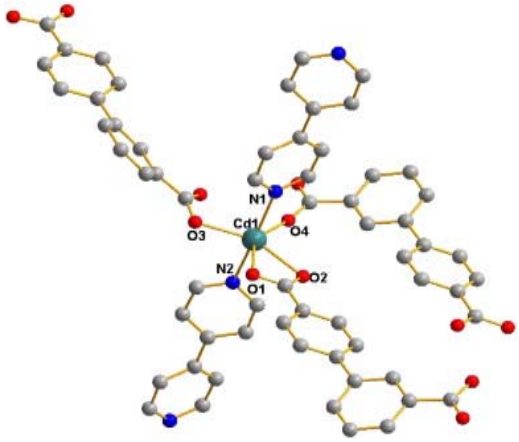

Figure 1.11 [Cd(bpdc)(bpy)·DMF] (bpdc=biphenyl-3,4′-dicarboxylic acid and bpy=4,4′-bipyridine) MOF that demonstrates flexibility in different solvents[14]

Molecular Separations

Column chromatography is a popular method of separating organic solvents and mixtures of larger molecules that can be dissolved in them. A MOF can be packed into a

HPLC column and used to separate organic molecules by properties such as polarity and size.[13] One particular example, the framework MIL-101(Cr) built of trimeric chromium clusters with terephthalate ligands (Fig 1.12), was used in a HPLC column to separate various substituted aromatic organic solvents.[6] A high selectivity for the *ortho*-isomers was found. This result is promising for future research on separation of molecules based on isomer types, and may even be applicable to biological molecules.[6]

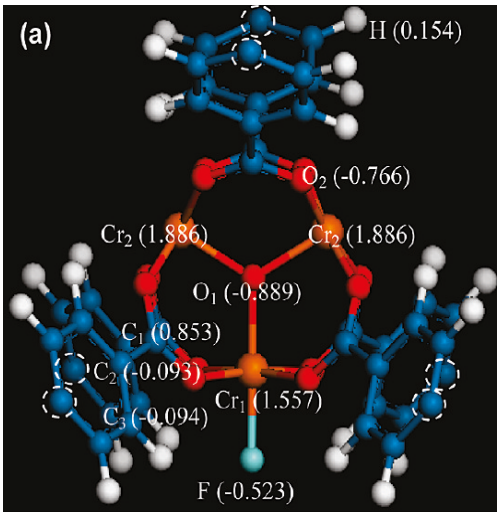

Fig 1.12 MIL-101(Cr) MOF[6]

Crystal to Crystal Guest Exchange

Crystal to crystal guest exchange happens when a layer of new solvent is placed over a thin layer of solvated crystal allowing for the adsorption of the new solvent.[12] In one particular example, the framework, $Zn_2NDC_2DPNI_2$ (NDC=1,6-napthalene dicarboxylic

acid and DPNI= N′,N-di-(4-pyridyl)1,4,5,8,-napthalene dicarboxylic acid) was solvated in DMF and exchanged with an equal volume of either chloroform, *n*-hexanol, or nitrobenzene.[12] It was found that with the presence of different solvents, structural changes in the MOF occurred. Another experiment tested the guest exchange of DMF with ethanol, methanol, and acetonitrile in the MOF [Cd(bpdc)(bpy)·DMF] (bpdc=biphenyl-3,4′-dicarboxylic acid and bpy= 4,4′-bipyridine).[14] No structural change was observed for this framework. Both of these experiments are useful for determining whether MOFs undergo guest induced structural changes and if so, whether they are able to return to their original structure after solvent induced structural changes occur.[14]

Water Adsorption

Along with organic solvents, water is also used for sorption studies. In one experiment, a MOF $[Cu(R\text{-}GLA\text{-}Me)(bpy)_{0.5}]\cdot 0.55\ H_2O$ (R-GLA-Me= R-methyl glutarate) was used to adsorb a binary 1:1 mixture of methanol and water.[9] Using larger R groups for the R-methyglutarate, the pores of the structure were reduced in size. The smaller dimension pore structure showed a strong preference for water adsorption over methanol. In another example, the 1D framework, $[Zn(HBTC)(DPE)_{0.5}(H_2O)]_n\cdot nH_2O$ (HBTC=dianion of 1,3,5-benzenetricarboxylic acid and DPE= 1,2-bis-(4-pyridyl)ethane) was thermally dehydrated into a new 2D framework, $[Zn(HBTC)(DPE)_{0.5}]_n$.[6] This second experiment is significant as it demonstrates H_2O ligand desorption.

Gas Sorption

Gas sorption is useful for the storage of small molecules such as H_2 and also beneficial for membrane-based gas separation.[11] The framework, $[Ni_2(bpy)_3(NO_3)_4]_n$ was used to study the adsorption characteristics of nitrogen, argon, carbon dioxide, and nitrous oxide gases, and ethanol and methanol vapors.[10] It was found that two processes are involved in adsorption: diffusion along the surface of the pores and diffusion through the barrier at the pore entrance and that either one of these could be a rate determining step.[10] Nitrogen, carbon dioxide, and nitrous oxide had the same rate determining step, which involved diffusion through the barrier at the MOF pore entrance. For methanol and ethanol vapors the rate determining step involved diffusion along the surface of the pores.[10]

$[Co_2(bpy)_3(NO_3)_4]_n$ Frameworks

The 2D bilayer MOF $[Co_2(bpy)_3(NO_3)_4]_n$ forms when crystals are grown from the components of cobalt nitrate and 4,4′- bipyridine in ethanol. The building blocks for the framework are T-shaped units made from the cobalt ion being connected by 4,4′-bipyridine ligands as shown in Fig 1.13. The properties of this MOF, including the factors controlling its growth and sorption properties were of interest. These T-shaped units have the ability to form different types of structures besides the 2D bilayer, including the 1D ladder and 3D brick wall (Figure 1.14).The crystals require only a few days to grow, which is faster than most other MOFs described in the literature. This makes it possible to make the large amounts of crystals needed for studying sorption properties.

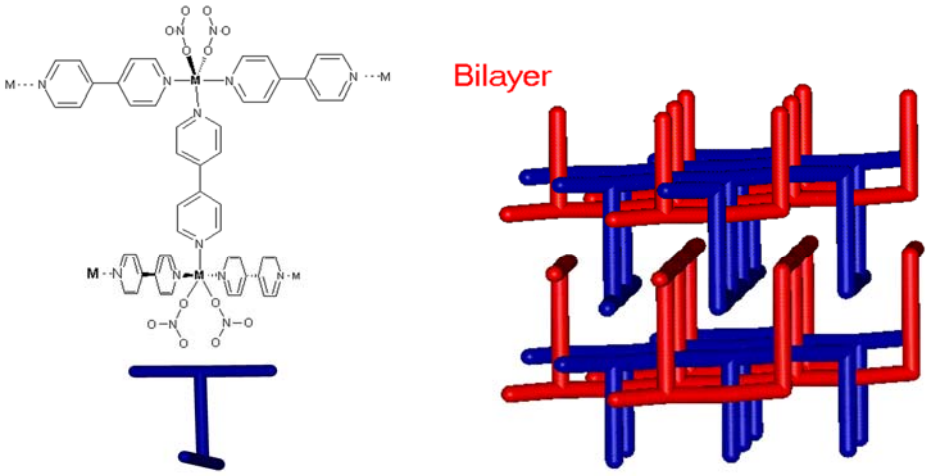

Fig 1.13 Diagram of the T-shaped unit and bilayer structure of $[Co_2(bpy)_3(NO_3)_4]_n$

Figure 1.14 Example of T-Shaped units used to build the 1D ladder (A) and 3D brick wall (B) of $[Co_2(bpy)_3(NO_3)_4]_n$

CHAPTER 2

EXPERIMENTAL

Materials

Materials used to synthesize the MOFs included: cobalt(II) nitrate hexahydrate (Alfa Aesar, 97.7%) , 4,4′-bipyridine (Acros, 98%), and ethanol (Acros, absolute 99.5% A.C.S. reagent, not denatured). Cobalt(II) nitrate hexahydrate was dried over anhydrous calcium sulfate prior to use. Other reagents were used as received. Vials for synthesis were 22 mL in volume with heights of 8.5 cm and diameters of 2.3 cm. Test tubes for synthesis were 22 mL in volume with heights of 14.5 cm and diameters of 1.2 cm.

Organic solvents used for adsorption studies included: ethanol (Acros, absolute 99.5%), 1-pentanol (Alfa Aesar 99%), toluene (Alpha Aesar spectrophotometric grade 99.7+%), cyclohexane (Fisher-Scientific 99.9%), and *n*-hexane (Alfa Aesar 99%).

Synthesis of $[Co_2(bpy)_3(NO_3)_4]_n$ Red Bilayer MOFs

Experiments were conducted to optimize the synthetic conditions to determine the most efficient method for producing large amounts of the red bilayer $[Co_2(bpy)_3(NO_3)_4]_n$ crystals for sorption studies (Figure 2.1). Cobalt(II) nitrate hexahydrate was carefully diffused with 4,4′-bipyridine (bpy) in ethanol solvent. Condition alterations included: changes in the concentration of the cobalt(II) nitrate hexahydrate and bpy solutions, changes in the volume of the middle ethanol layer that initially separated the cobalt(II) nitrate and bpy solutions, changes in the addition order of the layers, and changes in the temperature during layering of the solutions or during the slow diffusion process.

Figure 2.1 $[Co_2(bpy)_3(NO_3)_4]_n$ red crystals of the bilayer framework

Method 1

Dried cobalt(II) nitrate hexahydrate (0.019-0.11g) was dissolved in ethanol (2.0 mL). The samples were placed in a sonicator for 10 minutes to dissolve. Separately, bpy (0.010-0.11g) was also dissolved in ethanol (1.0-7.0 mL). The cobalt(II) nitrate solution vials were placed on ice, a layer of neat ethanol (5.0-12.0 mL) was added on top of the cobalt(II) nitrate solution, and finally the corresponding bpy solutions. The Co^{2+} to bpy ratio was either 1:2 or 2:3. The vials were carefully removed from the ice and left at room temperature for the framework building blocks to slowly diffuse together and form crystals. The ideal concentrations of cobalt(II) nitrate hexahydrate for organized red bilayer growth was approximately 0.10 g in 2.0 mL of ethanol, along with approximately 0.080 g of bpy dissolved in 7.0 mL of ethanol. The ethanol intermediate layer volume was 10.0 mL (height of approximately 3.0 cm). Red crystals would form, with the occasional unexpected formation of orange rectangular prism crystals (Figure 2.2). If concentrations of bpy and cobalt(II) nitrate hexahydrate solutions were greater than the

ideal amounts and if the ethanol intermediate layer volume was lower than 10.0 mL (less than 3.0 cm), clumps of powder and/or disorganized crystalline material would appear.

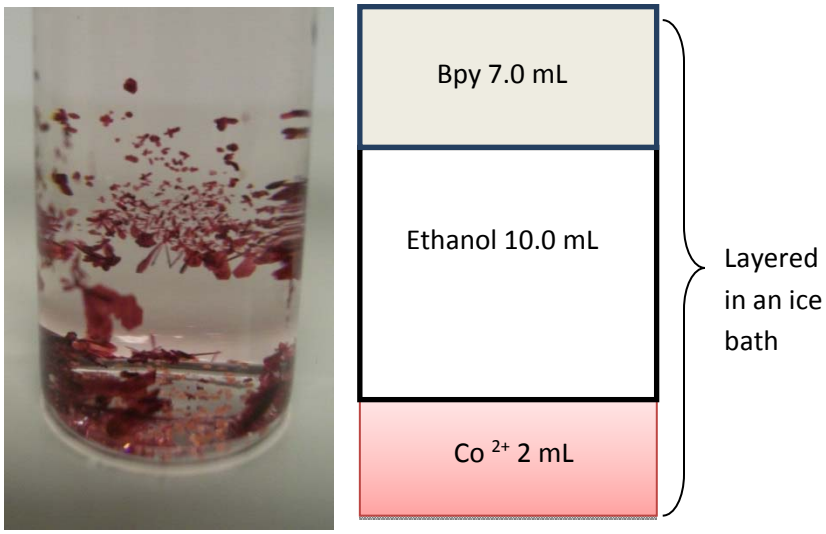

Figure 2.2 Mixture of $[Co_2(bpy)_3(NO_3)_4]_n$ red bilayer and rectangular prism orange crystals

Method 2

This experiment used a 2:3 ratio of cobalt nitrate to bpy. The vials had the 2.0 mL ethanol solution of cobalt(II) nitrate hexahydrate (0.020-0.051 g) layer at the top, with the 7.0 mL ethanol solution of bpy (0.016-0.040 g) on the bottom and a 10.0 mL intermediate ethanol layer. The bottom layers were cooled in an ice bucket before the addition of the other solution layers. Bilayer crystals formed as shown in Figure 2.3. Larger concentrations of cobalt(II) nitrate hexahydrate made the top solution too dense, causing it to sink and quickly mix with the bpy solution forming powder.

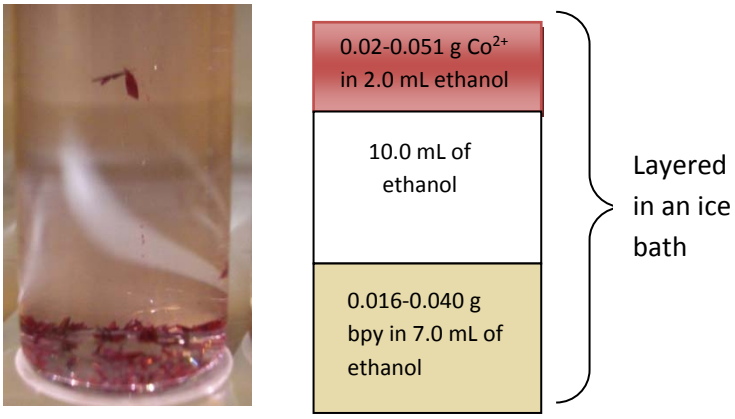

Fig 2.3 Crystal growth pattern with cobalt solution as the top layer

Method 3

This method involved a 2:3 ratio of cobalt nitrate to bpy using approximately 0.10 g of cobalt(II) nitrate hexahydrate dissolved in 2.0 mL of ethanol and 0.080 g of bpy dissolved in 7.0 mL of ethanol with a 10.0 mL ethanol intermediate layer. While these amounts are the same as the optimum values determined in Method 1, the layering of the bottom cobalt(II) nitrate solution, intermediate ethanol layer and top bpy solution layer was done at room temperature instead of in an ice bath. This method consistently formed long red needle crystals of the $[Co_2(bpy)_3(NO_3)_4]_n$ bilayer and did not result in the formation of orange rectangular prism crystals.

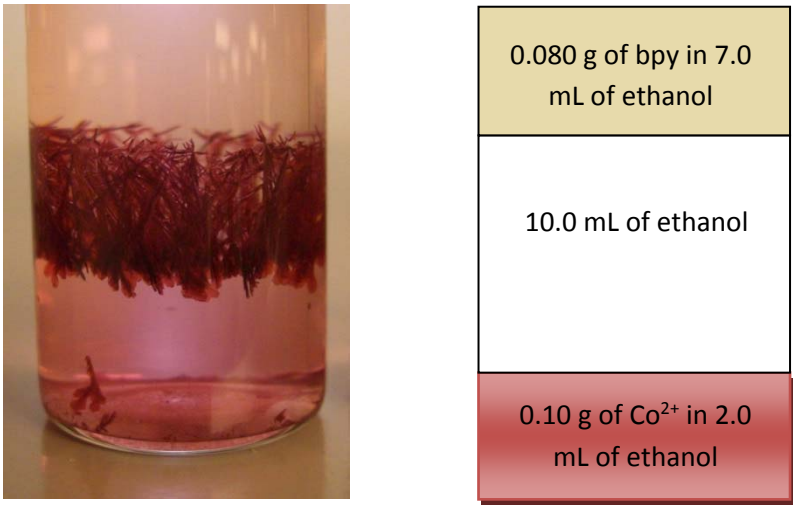

Figure 2.4 Elongated needles of the $[Co_2(bpy)_3(NO_3)_4]_n$ bilayer crystals formed from solutions layered at room temperature

Investigation of Orange 1D Chain MOFs

Using Method 1 of growing red bilayer crystals, unknown orange crystals would occasionally appear. Multiple experiments were conducted to prepare the orange crystals in pure form and to identify the factors that caused them to form.

Method A

In an attempt to seed the growth of orange crystals, a powdery mixture created by the rapid mixing of cobalt(II) nitrate hexahydrate (0.050-0.051g in 2.0 mL EtOH) and bpy (0.054-0.057 g in 7.0 mL EtOH) solutions was inserted into the intervening ethanol layer to test whether formation of orange crystals was triggered by some mixing of cobalt nitrate and bpy solutions during the layering of the solutions forming fine precipitates. The cobalt nitrate solution was on bottom and the bpy solution was on top and all

solutions were at room temperature. Both red and orange crystals formed, and no clear trend was observed. The hypothesis was tested further by carefully isolating orange and red crystals grown in previous experiments, grinding them up, making an ethanol suspension, and inserting this into the 10 mL ethanol layer in between the cobalt nitrate (0.050-0.102g in 2.0 mL ethanol) bottom solution and bpy (0.053-0.11 g in 7.0 mL ethanol) top solution as well. Using either the red $[Co_2(bpy)_3(NO_3)_4]_n$ bilayer or the orange seed crystals still resulted in mixtures of red and orange crystals forming.

Method B

The mole ratios of cobalt nitrate to bpy were altered to test if a local excess of one component during diffusion was a factor. Vials were set up at room temperature using a 2:3 or 1:3 ratio of Co:bpy (0.050-0.10 g of cobalt nitrate in 2.0 mL of ethanol, 10.0 mL intermediate ethanol layer, and 0.040-0.16g bpy in 7.0 mL of ethanol). The bpy solution was used as the top layer and the cobalt nitrate solution was used at the bottom layer. The 2:3 ratio did not form the orange crystals (though it had in previous experiments), the 1:3 ratio of higher concentrations (0.10 grams of cobalt(II) nitrate hexahydrate) formed orange and red crystals, but the 1:3 ratio of lower concentration (0.050 grams of cobalt(II) nitrate hexahydrate) formed red crystals and did not form orange crystals. Thus the ratio of framework building blocks and variation in solution concentration did not show a clear trend linked with the formation of the orange crystals.

Method C

An experiment was conducted to test whether the temperature at which the vials were kept while the reactants diffused together would affect crystal growth. In the past, it

appeared that orange crystals grew much more slowly, anywhere from 3 days to over a week, so it was predicted that cooling all the solutions prior to layering them in the vial would slow the process and result in orange crystals. Sixteen crystal growth vials were prepared and half of them contained approximately 0.10 g of cobalt nitrate hexahydrate and the other half contained 0.050 g. Each set of vials had the bpy in ethanol solution added with a Co:bpy ratio of 1:3 or 2:3. All cobalt nitrate solutions were in 2.0 mL of ethanol and used as the bottom layers. Also, all bpy solutions were in 7.0 mL of ethanol and used at the top layers. The intermediate ethanol layer was 10.0 mL. Half of the 0.10 g of the cobalt(II) nitrate hexahydrate solutions and half of the 0.050 g cobalt(II) nitrate hexahydrate solutions were placed in an ice bath to cool before combining components. The other vials and all the solutions to be layered in them were combined at room temperature. The observed trend was that long red needles tended to grow in vials that contained larger amounts of cobalt(II) nitrate hexahydrate. Also, orange crystals did not seem to appear in the vials prepared at room temperature, suggesting that temperature might be a factor in crystal formation.

Method D

To investigate the effects of temperature during the reactant diffusion process on orange crystal formation, solutions were placed in a cold room at approximately 0°C for 2 hours to ensure a homogenous temperature before layering in the vials. All vials had approximately 0.050 grams of cobalt(II) nitrate hexahydrate added. A quarter of the vials had a 2:3 ratio, a quarter had a 1:2 ratio, a quarter had a 1:3 ratio, and the remaining quarter had a 1:4 ratio. All cobalt(II) nitrate solutions were in 2.0 mL of ethanol and used

as the bottom layer. All bpy solutions were in 7.0 mL of ethanol and used as the top layer. The middle ethanol layer volume was 10.0 mL. All vials appeared the same with red bilayer crystals growing on the sides of the vial and an unidentified pink powder at the bottom. Also, the red bilayer crystals were much smaller in size, as shown in Figure 2.5.

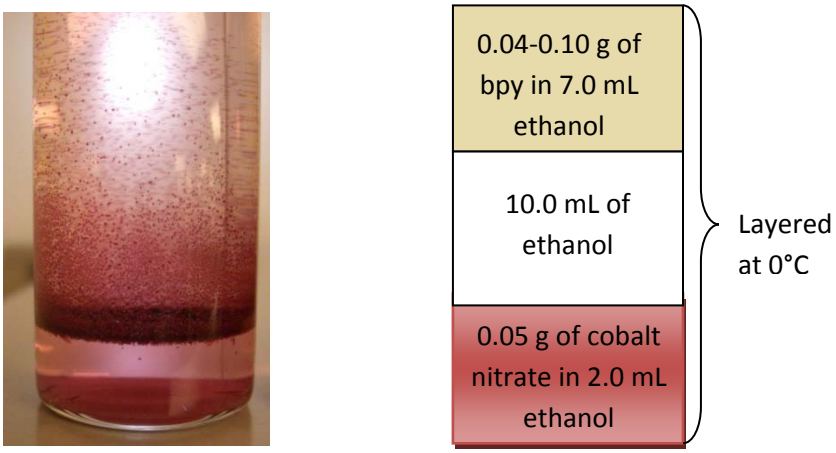

Fig 2.5 $[Co_2(bpy)_3(NO_3)_4]_n$ crystals grown in cold room at 0°C.

To further test the effects of temperature, crystals were grown in an oven. Approximately 0.049-0.052 g of cobalt(II) nitrate hexahydrate were dissolved in 2.0 ml of ethanol and 0.052-0.057 g of bpy were dissolved in 7.0 mL of ethanol. The cobalt(II) nitrate solution was the bottom layer. The bpy solution was layered on top of an intermediate layer of 10.0 mL ethanol within an ice bath. The vials were placed in an oven at 36°C. Mostly large red bilayer crystals appeared, but a few orange crystals also appeared in one of the vials.

Method E

This method was conducted to see if ethanol layer height affected orange crystal development. First, vials were prepared as normal using a 1:2 ratio of Co:bpy with approximately 0.050 g of cobalt(II) nitrate hexahydrate. Next, test tubes were utilized to create a longer ethanol layer distance between the solutions, containing the same 1:2 Co:bpy ratio with 0.050g of cobalt(II) nitrate hexahydrate. The cobalt(II) nitrate hexahydrate was dissolved in 2.0 mL of ethanol (used as the bottom layer) and the bpy was dissolved in 7.0 mL of ethanol (used at the top layer) along with an intervening layer of 10.0 mL of ethanol. The components were layered in an ice bath. Orange crystals appeared in only a few of the test tubes and there was not a clear relationship between the height/volume of the intervening ethanol layer and the formation of orange crystals.

Method F

This method was performed to further analyze ethanol layer height/volume and its effects on crystal growth. The method required a 2:3 Co:bpy ratio of 0.050 g of cobalt(II) nitrate hexahydrate dissolved in 2.0 mL of ethanol (used as the bottom layer) and 0.040 g of bpy dissolved in 7.0 mL of ethanol (used as the top layer) and involved altering the intermediate ethanol layer heights by using volumes of 12.0 mL, 14.0 mL, or 16.0 mL for the intermediate layer. Vials were also prepared using 12.0 mL of ethanol for the intermediate layer, but the cobalt nitrate was dissolved in 5.0 ml of ethanol first. A variation of this method used a 12.0 mL intermediate layer of ethanol with glass wool inserted below the bpy solution layer to inhibit solution mixing. Both red and orange crystals appeared in all situations.

Method G

Water was added to see if its presence affected the growth of orange crystals. Three vials were prepared at room temperature using a 2:3 ratio of Co:bpy with approximately 0.050 g of cobalt(II) nitrate hexahydrate dissolved in 2.0 mL of ethanol (used as the bottom layer), 0.040 g of bpy dissolved in 7.0 mL of ethanol (used as the top layer), and 10.0 mL of ethanol was used as the intermediate layer. The components were layered in an ice bath. The first vial had no added water, the second had 0.1 mL of water added on top of the ethanol layer, and the third vial had 0.2 mL of water added on top of the ethanol layer. Water seemed to cause the growth of the orange crystals. The vial with no added water contained only red bilayer crystals and the vials containing water had both red bilayer and orange crystals appear. To further analyze this, the experiment was repeated, systematically varying the volume of water in the range of 0.1-0.5 mL. It was found that vials with 0.5 ml of water (approximately 2.5% by volume) consistently produced only orange crystals (Figure 2.6).

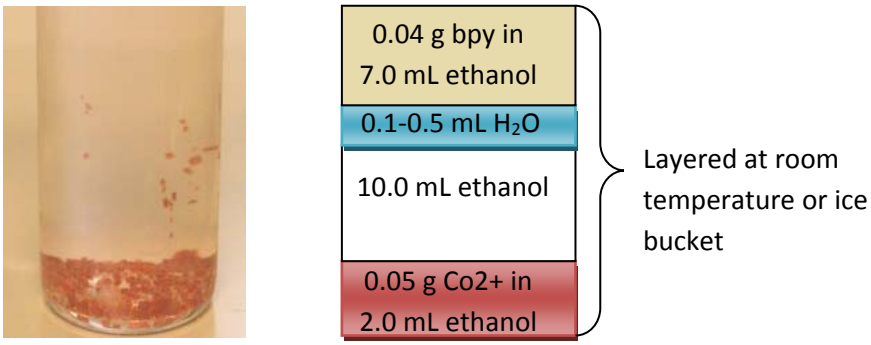

Figure 2.6 Orange crystals of $[Co(bpy)(NO_3)_2(H_2O)_2]_n$

Synthesis of Cobalt(II) Nitrate 4,4′-Bipyridine MOFs in which Red Crystals Disappeared and Were Replaced by Orange $[Co(bpy)(NO_3)_2(H_2O)_2]_n$ 1D Chain Crystals

Approximately 0.050 grams of cobalt(II) nitrate hexahydrate were dissolved in 2.0 mL of ethanol. On top of this solution, an ethanol layer of 10.0 mL was added. Additionally, between the bpy solution (approximately 0.040 grams bpy in 7 mL of ethanol) and ethanol intermediate layer, 0.5-0.7 mL of water were added. A mixture of red and orange crystals initially formed, changing over a period of a couple days to completely orange crystals.

Desolvation and Resolvation of $[Co_2(bpy)_3(NO_3)_4]_n$ Bilayer and $[Co(bpy)(NO_3)_2(H_2O)_2]_n$ 1D Chain MOFs

$[Co_2(bpy)_3(NO_3)_4]_n$ bilayer and $[Co(bpy)(NO_3)_2]_n$ orange 1D chain crystals were collected and placed in an oven (90°C) for about 3 hours to remove ethanol from the pores. Desolvation by drying in an oven at 90°C caused the transformation of the 1D chain crystals into new, purple crystals. Samples of each were collected in vials and placed in separate beakers filled either with water, ethanol, or acetonitrile and sealed with parafilm for at least a day and up to a month to see whether the solvent vapors would be adsorbed. With ethanol vapor resolvation, no apparent change in crystal shape or color was noticed for the bilayer or 1D chain crystals. However, acetonitrile resolvation caused the 1D chains to appear slightly dark red and water resolvation caused the transformation of the bilayer crystals to an orange powder. Water resolvation of the dried 1D chains was also conducted, changing them from purple crystals back to the original orange color, but in a more powdery form than the original crystals.

Single Crystal X-ray Diffraction of Orange $[Co(bpy)(NO_3)_2(H_2O)_2]_n$ 1D Chains and Dried $[Co(bpy)(NO_3)_2(H_2O)_2]_n$ 1D Chain MOFs

X-ray diffraction was performed at the Iowa State University in Ames, Iowa on the orange crystals grown in the ethanol/water solution and the purple crystals produced by drying them at 90°C. Selected crystals were less than a millimeter in size. An Apex II CCD X-ray detector was used. The structures were determined from the data using the XSHELL program and refined using SHELXTL.[22] OLEX2[23] was used to produce models of the structures and to calculate the solvent accessible volume of the pores in the $[Co(bpy)(NO_3)_2(H_2O)_2]_n$ 1D chain crystal structure.

Powder X-ray Diffraction of MOFs

A Rigaku Miniflex II Diaffractometer was used to obtain data on the structure of red bilayer crystals as synthesized, orange $[Co(bpy)(NO_3)_2(H_2O)_2]_n$ 1D chain crystals as synthesized, orange crystals that grew in diffusion reactions in which red crystals initially formed but the final product was orange crystals, purple dried 1D chain crystals, ethanol-resolvated bilayer crystals, acetonitrile-resolvated bilayer crystals, and water-resolvated bilayer crystals. Crystal samples were ground to a powder using a mortar and pestle and loaded onto a flat, round, aluminum sample holder. Collection parameters were: 2θ= 5°-55°, sampling ω= 0.050°, scan rate= 2°/min, v=20 kV, and I=15mA. The continuous sampling method was used. The program MDI Jade was used for data refinement to pick the peaks.

Elemental Analysis of MOFs

A Flash EA 2000 series instrument was used. The C, H, N compositions of the red bilayer, 1D $[Co(bpy)(NO_3)_2(H_2O)_2]_n$ orange chains, dried bilayer, dried 1D chains, water-resolvated bilayer, water-resolvated dried 1D chains, acetonitrile-resolvated bilayer, and acetonitrile-resolvated 1D chains were determined. The oven temperature was 950 ºC for the sample furnace. Argon carrier gas flow was 140 ml/min, oxygen flow was 250 ml/min and reference gas flow was 140ml/min. The cycle run time was 500 seconds. Aspartic acid was used as a standard.

IR Spectroscopy of MOFs

IR spectra were recorded using a Nicolet IR200 FTIR spectrometer and the OMNIC program was used for data collection and peak indentification. Dried bilayer, dried 1D chains, water-resolvated 1D chains, orange $[Co(bpy)(NO_3)_2(H_2O)_2]_n$ 1D chains, bilayer in EtOH, water-resolvated bilayer, acetonitrile-resolvated bilayer, acetonitrile-resolvated 1D chains, ethanol-resolvated bilayer, and ethanol-resolvated 1D chains were analyzed. Samples were ground to a powder using a mortar and pestle. Spectra were collected using an ATR sample holder and 16 scans were collected for each sample using a resolution of 4 cm^{-1}.

Thermogravimetric Analysis (TGA) of MOFs

Thermogravimetric analyses were performed using the TGA SDTA 851e instrument. Samples were placed in a 40 μL aluminum pan. The samples were held at 25°C for 2

min, heated to 125°C at 5°C/min, then heated to 500°C at 10°C/min, and held at 500°C for 15 min. The purge gas was nitrogen and the flow rate was 60-80 mL/min.

Liquid Sorption Studies on the Bilayer using a GC-MS

The results of liquid adsorption studies on the red 2D bilayer crystals of $[Co_2(bpy)_3(NO_3)_4]_n$ were quantified using a Shimadzu GC-17A with a flame ionization detector.\. The temperature program used was: Segment 1: Temperature= 40°C, Wait= 2.0 min, Segment 2: Rate= 10.0°C/min, Final Temperature= 225°C, and Wait= 5.0 min. The column was a 15 m Alltech At-225. The composition data was used to determine if the bilayer crystals had affinities to different guest molecules.

Method 1

Standard concentrations of 10%, 5%, 2%, and 1% ethanol in 1-propanol with a toluene internal standard were prepared. About 0.3 g of MOF crystals were added to 5 mL of 1-propanol in a 25 mL round bottom flask with a magnetic stirrer. Multiple 0.2 mL extractions were collected over 2 hours and added to vials containing 0.2 mL toluene as an internal standard.

Method 2

Experiments were performed using 50/50 v/v combinations of ethanol/toluene, toluene/cyclohexane, ethanol/1-pentanol, and toluene/*n*-hexane. GC peaks were well separated from each other for all components, so it was determined that these combinations would be acceptable for use in adsorption studies. Vials were obtained (12 mL) and 4.0 mL of both designated solvents were added to prepare each 8.0 mL binary

solution. Next, 2.0 mL from each of the 50/50 v/v solvents were added to one of four 6 mL sample vials containing a dried sample of the $[Co_2(bpy)_3(NO_3)_4]_n$ dried bilayer crystals of approximately 0.3 grams. Aliquots were taken and immediately measured using the gas chromatograph at time points varying over several hours or several days. Multiple measurements of the MOF-free control solutions were taken as well.

CHAPTER 3

RESULTS AND DISCUSSION

Crystal Growth Methods

Several variations of the methods for growing MOFs were used to produce the red bilayer crystals and also resulted in the findings of two new crystal structures, the orange crystals and the purple crystals produced by drying them. The ideal conditions for consistently growing the red bilayer crystals involved a 2:3 ratio of Co:bpy using 0.10 g of cobalt(II) nitrate hexahydrate dissolved in 2.0 mL of ethanol (bottom layer), 0.08 g of bpy dissolved in 7.0 mL of ethanol (top layer), and a 10.0 mL ethanol intermediate layer with all components layered at room temperature. This method worked the best due to large crystal yield without unwanted powder formation.

The ideal conditions for consistently producing orange crystals required a 2:3 ratio of Co:bpy using 0.050 g of cobalt(II) nitrate hexahydrate dissolved in 2.0 mL of ethanol (bottom layer), 0.040 g of bpy dissolved in 7.0 mL of ethanol (top layer), 10.0 mL of ethanol for the intermediate layer, and 0.1-0.4 mL of water in-between the ethanol and bpy layers. This method worked the best as using larger amounts of water would occasionally form red bilayer crystals which would take over a week to disappear and be replaced by orange 1D chain crystals (Figure 3.1). The orange 1D chain crystals were originally produced due to water vapor from the humid air condensing in the cold solutions when they were layered in an ice bath. This explained the confusion involved during initial experimentation when both red and orange crystals formed, but inconsistently. The inconsistency was due to the day to day variation in the weather.

A: Vial after 2 days B: Vial after 5 days

C: Vial after 7 days D: Vial after 9 days

Figure 3.1 Initial formation of red crystals followed by their disappearance and the growth of orange crystals

Vapor Sorption Methods

Vapor resorption experiments suggested that acetonitrile and ethanol did not alter the Co^{2+} coordination of the red bilayer crystals and 1D chain crystals. However, water vapor always seemed to interact with the structures of both the red bilayer and 1D chain crystals. Dried red bilayer crystals changed into an orange color and lost their single crystallinity as well upon water vapor resolvation (Figure 3.2). Purple crystals with intact

1D chains formed when orange 1D chain crystals were dried (Figure 3.3 A). However, they did not retain single crystallinity upon water vapor resolvation (Figure 3.3 B).

A  B  C 

Figure 3.2 Dried bilayer crystals (A), bilayer crystals after water vapor sorption (B), and a zoomed in view of the powdery water-resolvated bilayer (C)

A  B 

Figure 3.3 Zoomed in view of the dried 1D chain crystals (A) and water resolvation of dried $[Co(bpy)(NO_3)_2(H_2O)_2]_n$ 1D chain crystals (B)

Single Crystal X-ray Diffraction

Dr. Arkady Ellern and Dr. Colin Weeks solved the structure of the orange crystals using direct methods and determined that they were a new structure with infinite 1D chains of Co-bpy (Figure 3.1). It was observed that two pyridyl groups, two nitrates, and two water molecules were bound to the cobalt atom. Since water was a ligand, it was then concluded that water must have accidentally entered the vials due to condensation from the air, which was enhanced by the cooling of the vials in an ice bath while layering the solutions on top of each other. This was demonstrated in the crystal growth methods when both red bilayer and orange 1D chain crystals formed at the same time.

Table 3.1 Single crystal x-ray diffraction data on orange crystals

Formula of the refinement model	$C_5H_6Co_{0.5}N_2O_4$
Formula weight	187.58
Crystal color, habit	orange, prism
Crystal dimensions	0.30 x 0.30 x 0.30 mm
Crystal system	orthorhombic
Space group	*Pccn*
a	11.7636(14) Å
b	19.487(2) Å
c	7.3919(9) Å
V	1694.5(4)Å^3
D_c	1.47 g cm^{-3}
Z	8
$2\Theta_{max}$	28.700
hkl range	-15 15, -25 26, -9 9
N	16333
N_{ind}	2180
N_{obs}	2008
N_{var}	115
Residuals: R, Rw	0.0626, 0.1814
GoF	1.302

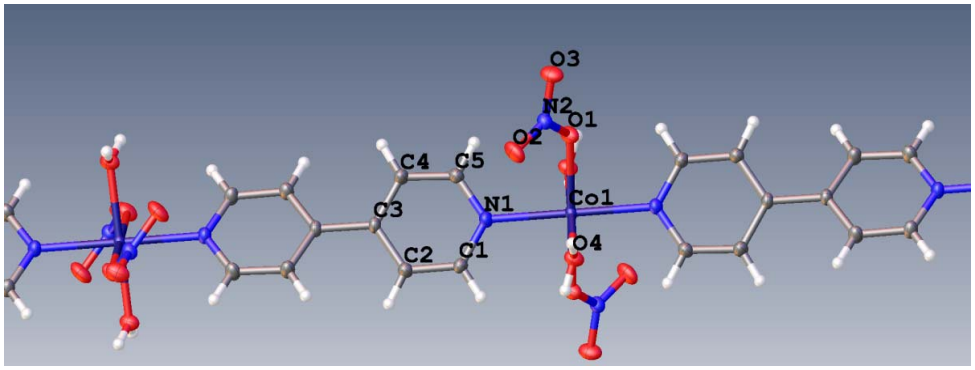

Figure 3.4 1D chain structure of the orange crystals

These 1D chains pack into in the crystal in layers. The chains in each layer are parallel, and the chains in alternate layers run in different directions (Figure 3.5 A). Small holes form within the layers which are capable of containing solvent. Figure 3.5 B shows the solvent accessible volume within the shaded structures. Figure 3.6 shows hydrogen bonding occurring between the hydrogen of the water ligand and the oxygen of the nitrate. Two types of bonding occur. The first is shown in Figure 3.6 A and occurs in chains two layers apart running in the same direction. The second occurs between chains in adjacent layers that run in opposite directions (Figure 3.6 B). These hydrogen bonds are what stabilize the stacking of the chains and the porous structure.

After obtaining and refining the purple dried 1D chain structure using the program SHELXTL, the results were still not entirely conclusive (Figure 3.7). The asymmetric unit seems to have two nitrate ligands and there is electron density at the other two coordination sites (modeled as O atoms) but the positions of these ligands are disordered and cannot be clearly modeled as aqua ligands. It is known that the structure is still a 1D

chain, and the bpy ligands are easily located, but it has not been possible to fully model the disorder of the nitrate ligands.

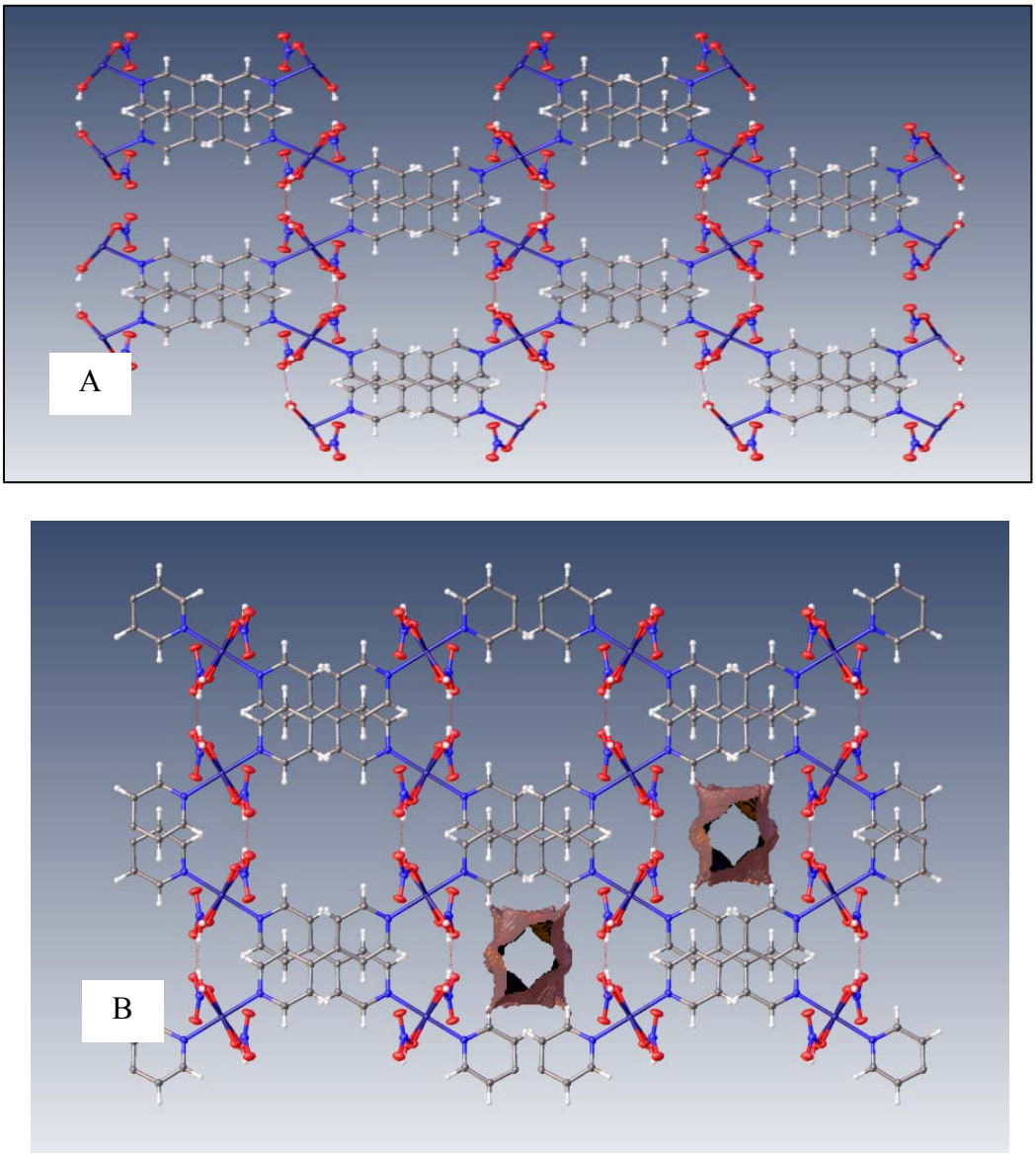

Figure 3.5 1D chains running in different directions in alternate layers (A) and void volumes in the orange 1D chain pores filled with solvent (B)

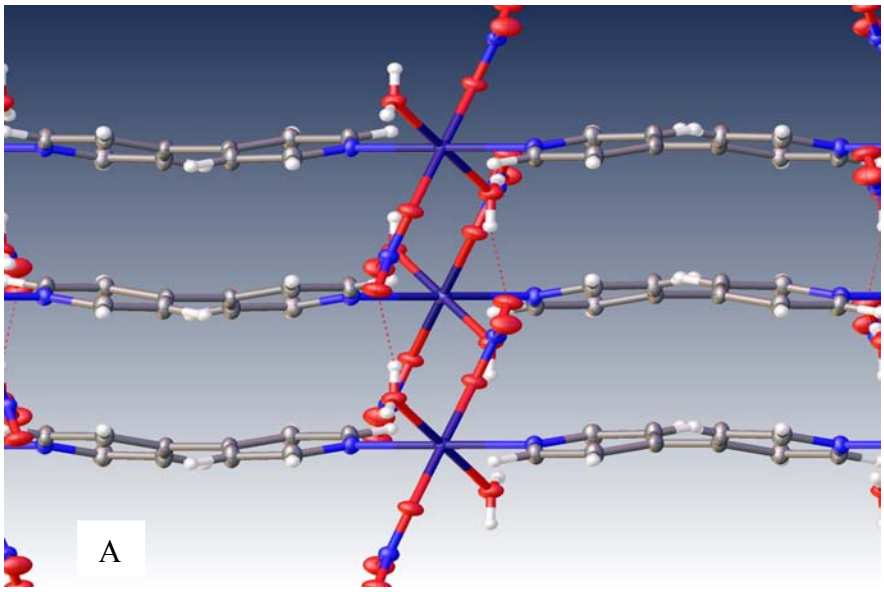

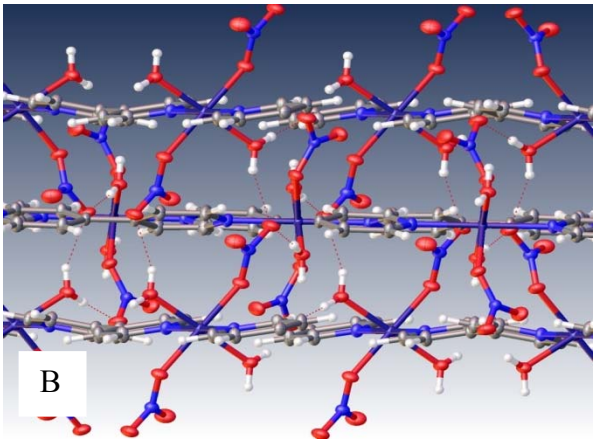

Figure 3.6 Hydrogen bonding within the orange 1D chain pores (A) and (B)

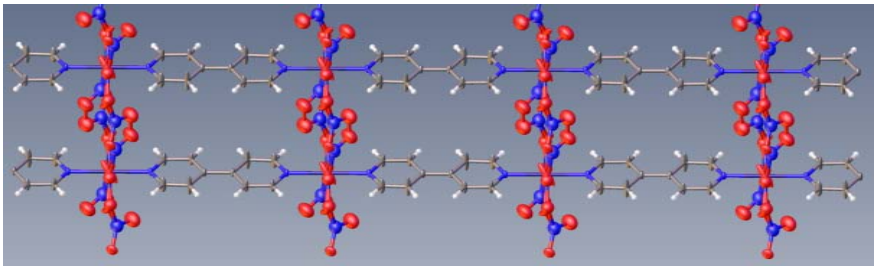

Fig 3.7 Structure of dried 1D chain crystals

Powder X-ray Diffraction

The PXRD patterns of the as-synthesized red bilayer and orange 1D chain crystals were measured along with the dried bilayer, ethanol-resolvated bilayer, acetonitrile-resolvated bilayer, dried 1D chain, ethanol-resolvated 1D chains, and acetonitrile-resolvated 1D chain crystals. The results showed that the structures of the dried bilayer crystals were similar to their corresponding ethanol-soaked crystals, but had slightly different peak intensities (Figure 3.8). Peak shifts were apparent in the dried bilayer at smaller 2Θ values and also new peaks were observed between 10-15° 2Θ that disappeared in the ethanol-resolvated sample The peaks for the ethanol-resolvated bilayer crystals perfectly matched the original bilayer in ethanol (Figure 3.8). Figure 3.9 shows the red bilayer crystals resolvated with both water and acetonitrile. The acetonitrile resolvated bilayer closely matches the bilayer in ethanol as synthesized, suggesting that the acetonitrile enters the pores of the structure but does not interact with the framework. The water resolvated bilayer has more peaks than the synthesized bilayer showing that water interacts with the framework. These major peak intensity and position differences correlate with the color changes observed. The color change is probably caused by a change in cobalt coordination. Figure 3.10 shows the PXRD peak patterns for the orange 1D chain and desolvated purple 1D chain crystals. The dissimilarities in peak intensities for the 1D chain crystal structures show that they are indeed different in structure. This confirmed the single crystal XRD data from Figures 3.4 and 3.7 which suggested that water ligands were absent in the desolvated purple 1D chain crystals. Figure 3.11 showed that the orange crystals that replaced the red crystals in the experiment with 0.5-

0.7 mL of water added were the 1D chain crystal structure. In Figure 3.12, orange 1D chain crystals as synthesized are compared to acetonitrile-resolvated 1D chain crystals and water-resolvated 1D chain crystals. The water-resolvated 1D chain crystals seem to be the exact same structure as the orange 1D chain as synthesized crystals. The acetonitrile-resolvated 1D chain crystals have some similar peaks as well to the as-synthesized 1D chain crystals, but these peaks appear to be broader suggesting a lower degree of crystallinity and the peaks observed indicate the presence of a mixture of desolvated 1D chain crystals and resolvated 1D chain crystals.

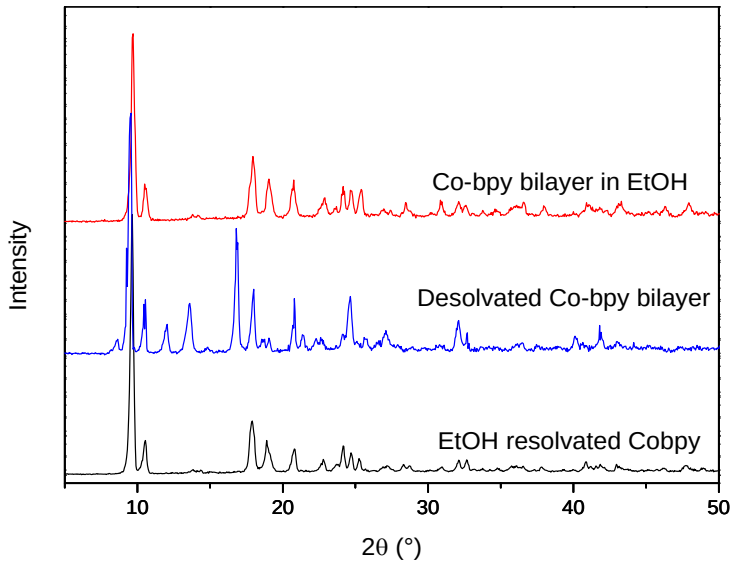

Figure 3.8: PXRD results from bilayer in EtOH, dried bilayer, EtOH resolvated bilayer

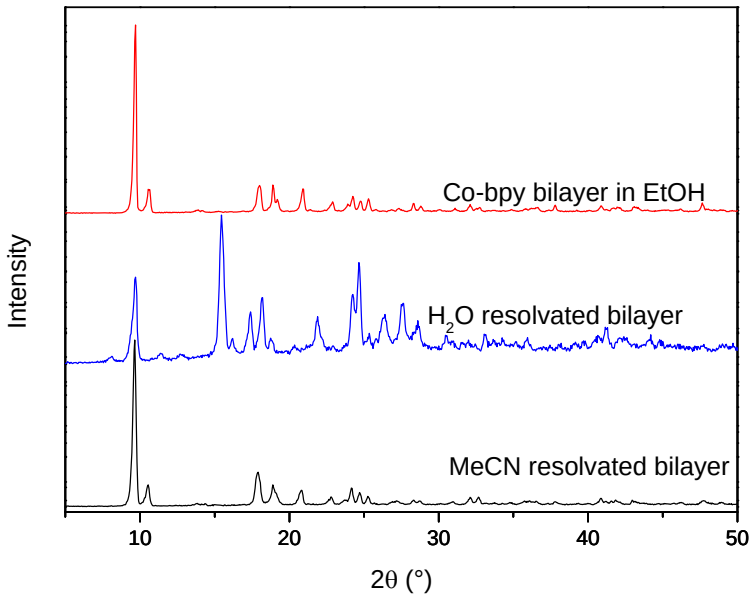

Figure 3.9 Bilayer as synthesized, water resolvated bilayer, and acetonitrile resolvated bilayer

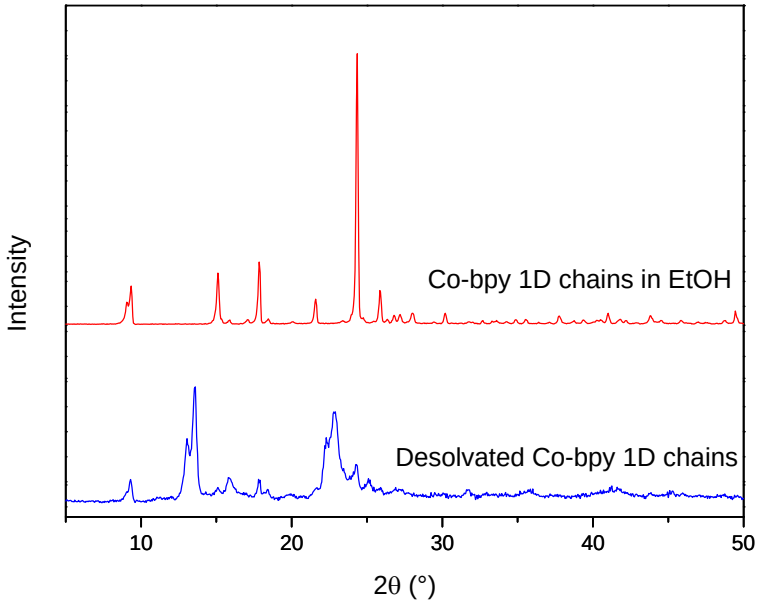

Figure 3.10 Orange 1D chain crystals and dried purple 1D chain crystals

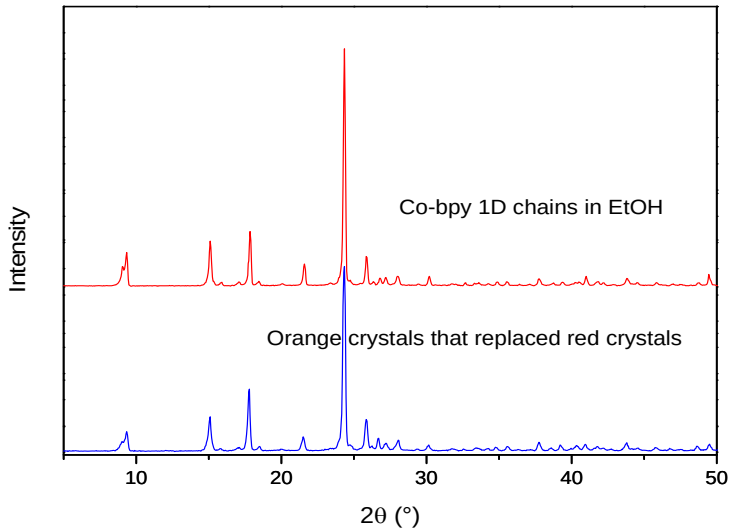

Figure 3.11 PXRD of orange 1D chains as synthesized compared to the crystals that changed from red to orange using conditions with larger amounts of water

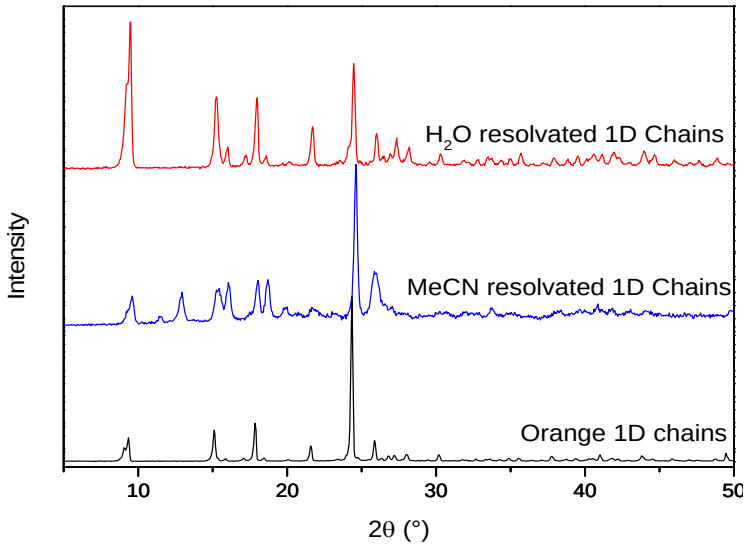

Figure 3.12 PXRD of orange 1D chains as synthesized compared to acetonitrile and water-resolvated 1D chains

IR Spectroscopy

The IR spectra for the red bilayer and orange 1D chain crystals are shown in Figures 3.13-3.22. The differences in the graphs are due to either the presence or absence of OH stretching peaks. The OH stretching peak located at 3300 cm^{-1} in the red bilayer crystals as synthesized (Figure 3.13) is due to ethanol as it completely disappears when the red bilayer crystals are dried at 90°C (Figure 3.14). This indicates that all the ethanol is removed from the pores when the crystals are dried. The rehydrated bilayer crystals have a much broader OH stretching peak at almost 100 cm^{-1} lower at 3198 cm^{-1} which indicates the presence of water molecules instead of ethanol (Figure 3.15). It is likely that the water molecules are binding to the cobalt atom. Figure 3.16 shows the spectrum of acetonitrile-resolvated bilayer crystals which lack OH peaks as expected due to the absence of both ethanol and water. However, the OH stretching peaks in the ethanol vapor resolvated bilayer crystals was much weaker than in the original sample (Figure 3.17). This indicates that resolvation of the crystals was incomplete.

There is a broad OH peak in the 1D chain crystals as synthesized graph at 3319 cm^{-1} (Figure 3.18) due to water and ethanol in the pores and the aqua ligands bound to the cobalt atom s. This peak disappears when the 1D chain crystals are dried (Figure 3.19) except for a small remaining hill in the same area suggesting that some water might still be coordinated to the metal. A strong water peak returns at 3210 cm^{-1} in the water-resolvated 1D chain crystal sample (Figure 3.20). This peak could be attributed to water in the pores and/or coordinated aqua ligands. The acetonitrile-resolvated 1D chain crystals have an unexpected OH peak (Figure 3.21). This must have appeared due to

humidity of the air during measurement. The ethanol-resolvated dried 1D chain crystals also have a strong OH peak attributed to ethanol in the pores (Figure 3.22).

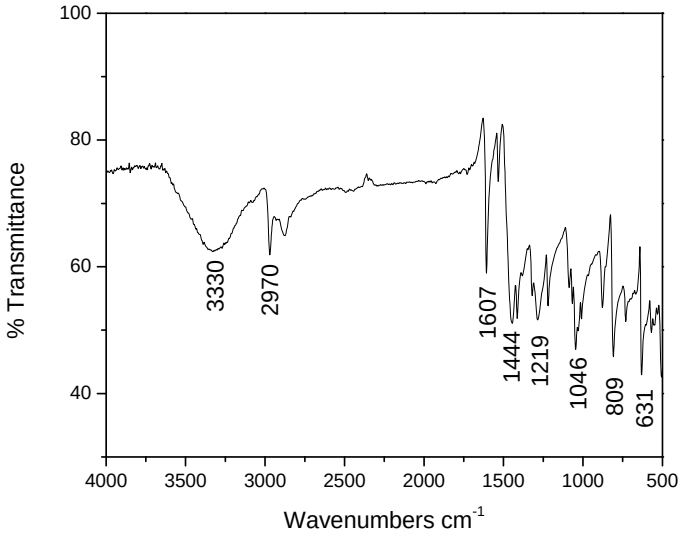

Wavenumber	Functional Group
3300 cm^{-1}	OH stretch
1607 cm^{-1}	Pyridyl Ring
1444 cm^{-1}	Pyridyl Ring

Figure 3.13 IR spectrum of bilayer in ethanol as synthesized

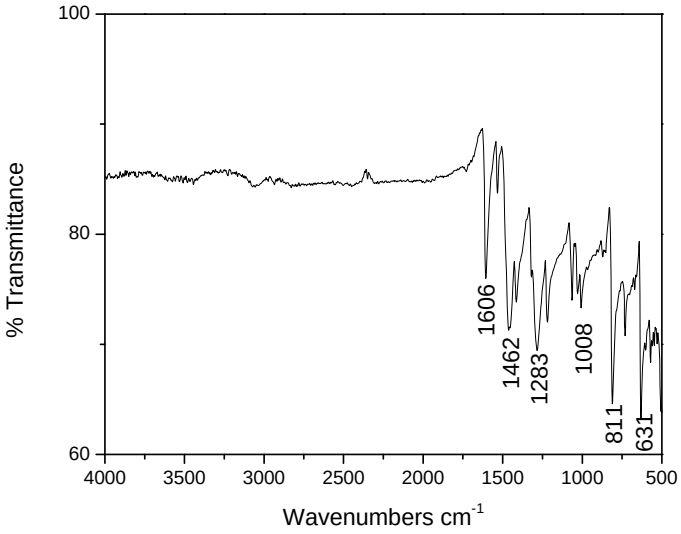

Wavenumber	Functional Group
1606 cm^{-1}	Pyridyl Ring
1438 cm^{-1}	Pyridyl Ring

Figure 3.14 IR spectrum of dried bilayer crystals

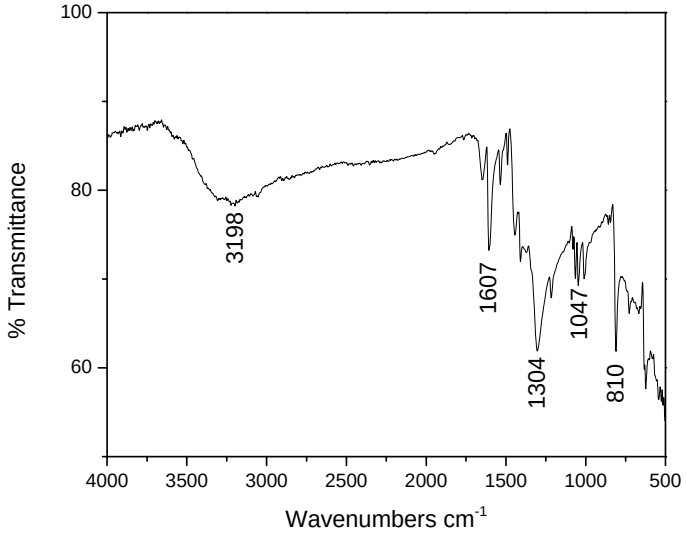

Wavenumber	Functional Group
3198 cm^{-1}	OH stretch
1607 cm^{-1}	Pyridyl Ring

Figure 3.15 IR spectrum of water-resolvated bilayer crystals

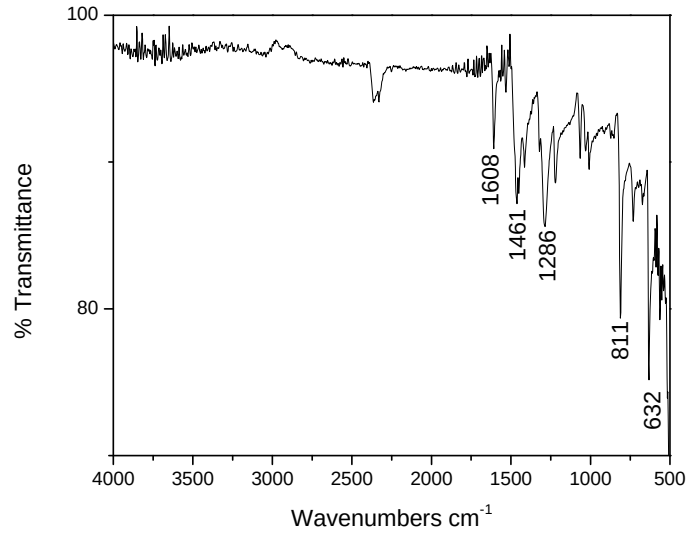

Wavenumber	Functional Group
1608 cm^{-1}	Pyridyl Ring
1461 cm^{-1}	Pyridyl Ring

Figure 3.16 IR spectrum of acetonitrile-resolvated bilayer crystals

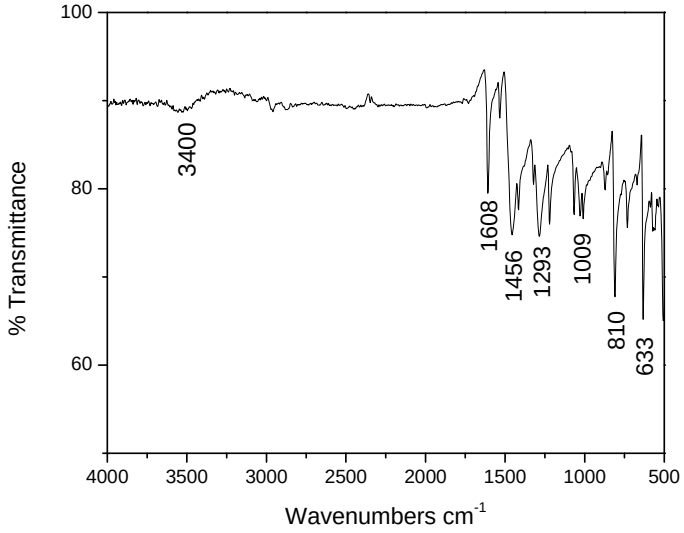

Wavenumber	Functional Group
1608 cm^{-1}	Pyridyl Ring
1456 cm^{-1}	Pyridyl Ring

Figure 3.17 IR spectrum of ethanol-resolvated bilayer crystals

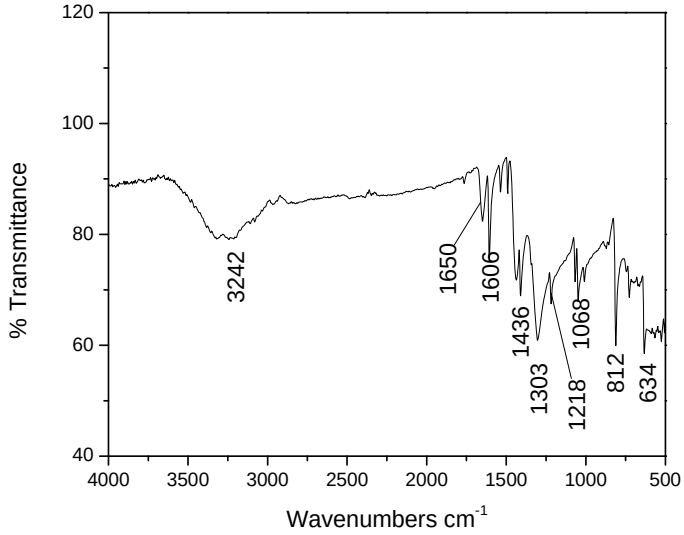

Wavenumber	Functional Group
3319 cm^{-1}	OH stretch
1648 cm^{-1} and 1606 cm^{-1}	Pyridyl Ring

Figure 3.18 IR spectrum of orange 1D chain crystals as synthesized

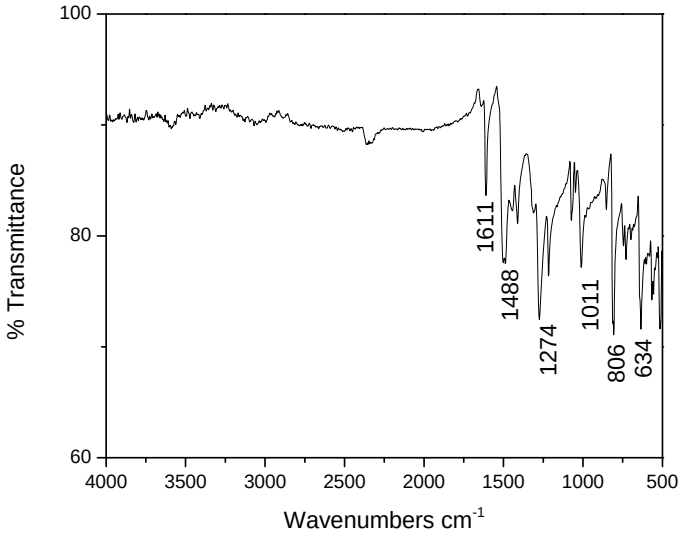

Wavenumber	Functional Group
1611 cm^{-1} and 1488 cm^{-1}	Pyridyl Ring

Figure 3.19 IR spectrum of dried 1D chain crystals

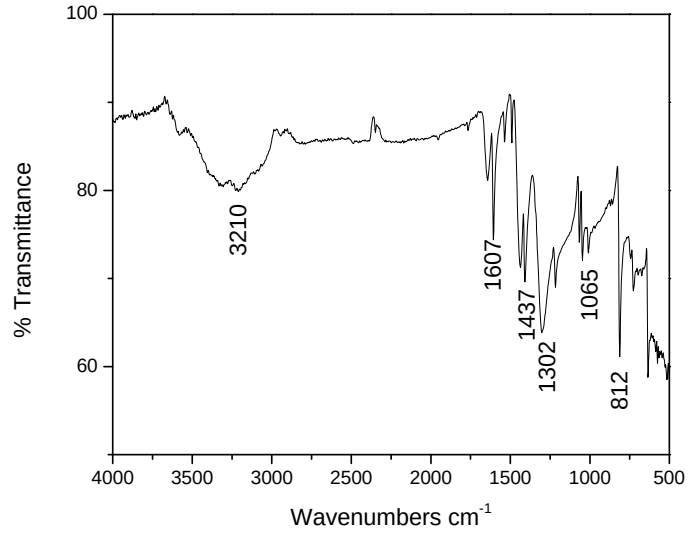

Wavenumber	Functional Group
3210 cm^{-1}	OH
1607 cm^{-1}	Pyridyl Ring
1437 cm^{-1}	Pyridyl Ring

Figure 3.20 IR spectrum of water-resolvated 1D chain crystals

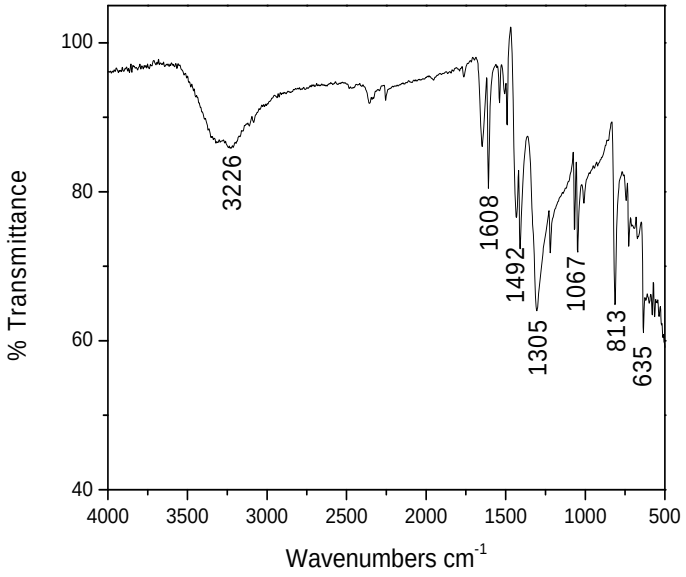

Wavenumber	Functional Group
3226 cm^{-1}	OH stretch
1608 cm^{-1}	Pyridyl Ring
1492 cm^{-1}	Pyridyl Ring
1305 cm^{-1}	Pyridyl Ring

Figure 3.21 IR spectrum of acetonitrile-resolvated 1D chain crystals

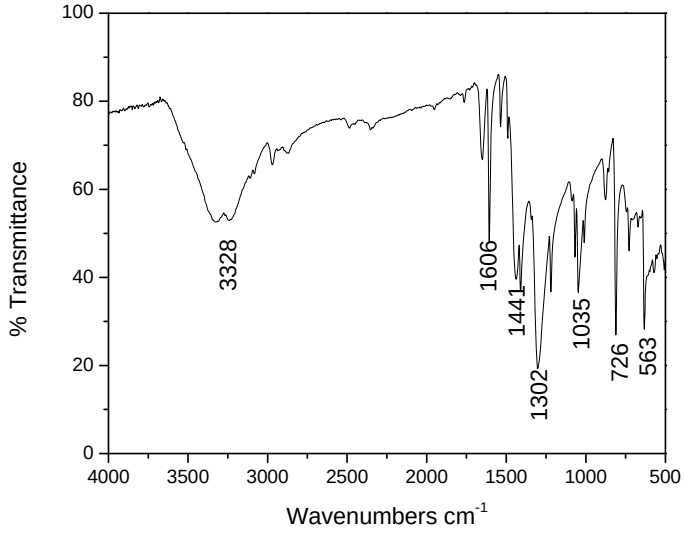

Wavenumber	Functional Group
3307 cm^{-1}	OH
1603 cm^{-1}	Pyridiyl Ring
1441 cm^{-1}	Pyridyl Ring

Figure 3.22 IR spectrum of ethanol-resolvated 1D chain crystals

Elemental Analysis

The percent composition of nitrogen, carbon, and hydrogen were obtained for each sample (Table 3.2). Calculations using different combinations of framework, water, ethanol, and acetonitrile molecules as necessary were performed to estimate the chemical formulas of the samples (Table 3.3). The molecular weights used were: Co= 58.933 g/mol, C=12.011 g/mol, N=14.007 g/mol, H=1.008 g/mol, and O=15.999 g/mol. The molecular formulas of the frameworks were $Co_2C_{30}H_{24}N_{10}O_{12}$ for the red bilayer and $CoC_{10}H_{12}N_4O_8$ for the 1D chain crystals.

The red bilayer framework with one and a half molecules of ethanol and one water molecule was closest to the C, H, N experimental percent composition values for the red bilayer crystals as synthesized. The dried bilayer crystals were calculated to be equivalent to one red bilayer framework molecule with no solvent in the pores. The water-resolvated bilayer crystals were calculated to be equal to one molecule of the red bilayer framework with the addition of twelve molecules of water. The acetonitrile-resolvated bilayer crystals consisted of one red bilayer framework molecule with one acetonitrile molecule and two water molecules. The reason for the presence of the calculated water molecules within the synthesized red bilayer crystals was due to the use of the hexhydrate salt of cobalt(II) nitrate in the synthesis and in the acetonitrile-resolvated bilayer crystals could be attributed to the adsorption of humidity in the air in the vessel set up for the vapor diffusion experiment. These results showed that the dried bilayer structure had a strong affinity for water.

A 1D chain framework molecule with one molecule of ethanol and one molecule of water was calculated to match the 1D chain crystals as synthesized based on C, H, N composition values. The 1D chain framework molecule along with the subtraction of two water molecules was assigned to the dried 1D chain crystals. The removal of water molecules from the 1D chain framework formula to match the experimental data suggested that the two aqua ligands were removed to form the dried 1D chain crystals. This shows that the two aqua ligands are readily removed from the framework as the sample was dried simply by heating at 90°C. This also explains why the nitrate ligands are disordered in the SCXRD (single crystal x-ray diffraction) structure of the dried 1D chain crystals. A 1D chain framework molecule with restored aqua ligands, the addition of four water molecules in the pores was assigned to the water-resolvated 1D chain crystals. Also, a 1D framework molecule with one molecule of water was assigned to the acetonitrile-resolvated 1D chain crystals. This showed that MeCN vapor did not enter the pores of the dried crystals, but the structure has a high affinity for water vapor and adsorbed it from humidity in the air of the MeCN vapor chamber. The addition of the water molecule to the 1D chain framework molecule to match the acetonitrile-resolvated 1D chain crystal percent composition values suggested that acetonitrile was not actually entering the pores of the 1D chain crystals.

Table 3.2 Experimental Elemental Analysis C, H, N Data

Sample Name:	% C	% H	% N
Red bilayer crystals in ethanol	42.94	3.63	14.94
Dried red bilayer crystals	42.67	2.85	16.45
Water-resolvated bilayer crystals	34.43	3.77	12.97
Acetonitrile-resolvated bilayer crystals	42.81	3.30	16.03
1D chains in ethanol	33.28	3.89	13.52
1D chains dried	35.53	2.36	16.33
1D chains H2O vapor	29.90	3.42	13.13
1D chains MeCN vapor	32.81	3.64	14.061

Table 3.3 Calculated C, H, N Composition for Framework and Solvent in the Pores

Possible Sample Compositions:	%C	%H	%N	Sample Experimental C, H, N Data Matches	Calculated % Mass of Solvent in Pores
Bilayer+1 water	42.27	3.07	16.43		
Bilayer +2 water	41.39	3.24	16.09		
Bilayer +1 EtOH	43.65	3.43	15.91		
Bilayer +2 EtOH	44.07	3.91	15.12		
Bilayer +2 EtOH +1 water	43.23	4.06	14.83		
Bilayer + 1.5 EtOH + 1 water	**43.01**	**3.83**	**15.20**	**Bilayer in EtOH**	**9.45%**
Bilayer +1 EtOH +1 water	42.72	3.59	15.59		
Bilayer +1 EtOH+ 2 water	41.93	3.74	15.28		
Bilayer	**43.18**	**2.9**	**16.79**	**Dried Bilayer**	**0%**
Bilayer +7 water	37.51	3.99	14.58		
Bilayer + 10 water	35.5	4.37	13.81		
Bilayer + 12 water	**34.3**	**4.61**	**13.33**	**Bilayer + water vapor**	**20.58%**
Bilayer+ 1 MeCN	43.9	3.12	17.6		
Bilayer +2 MeCn	44.56	3.3	18.33		
Bilayer +1 MeCN+ 1 water	43.02	3.27	17.24		
Bilayer +1 MeCN+ 2 water	**42.17**	**3.42**	**16.9**	**Bilayer resolvated with MeCN vapor**	**8.47%**
1D chain	34.6	3.48	16.14		
1D chain +1 EtOH	36.65	4.61	14.25		
1D chain +0.5 EtOH + 1 water	31.7	4.05	13.46		
1D chain + 1 EtOH + 1 water	**32.81**	**4.59**	**12.76**	**1D chain in EtOH**	**20.97%**
1D chain - 1 water ligand	33.6	2.82	15.67		
1D chain - 2 water ligands	**35.39**	**2.38**	**16.51**	**Dried 1D chains**	**n/a**
1D chain + 1 MeCN + 1 water	35.48	4.22	17.32		
1D chain + 1 water	**30.55**	**3.59**	**14.25**	**1D chain resolvated with MeCN vapor**	**11.71%**
1D chain + 3 water	4.52	4.52	13.97		
1D chain + 4 water	**28.65**	**4.81**	**13.43**	**1D chain resolvated with water vapor**	**17.19%**

Thermogravimetric Analysis

Thermogravimetric analysis was used to determine the temperatures at which the crystal frameworks decomposed and the mass percent of solvent lost from the pores. Data for the red bilayer crystals showed that solvent mass was immediately lost for the red bilayer crystals in ethanol, with approximately 20% of the total sample mass before the temperature reached 80°C (Figure 3.23). This was larger than the amount of solvent calculated from the elemental analysis data in Table 3.3 (solvent loss of 9.45%). This was attributed to loss of ethanol from the crystals during the longer sample preparation for the C, H, N analysis. As expected, the dried red bilayer crystals did not show any evidence of solvent loss (Figure 3.24), matching the elemental analysis data of 0% solvent loss in Table 3.3. For the water-resolvated bilayer, water did not start evaporating (about 25% of the sample mass) until approximately 100°C (Figure 3.25). There are a few small steps on the graph during the water evaporation. A step near 100°C is most likely due to the loss of the water in the pores and another prominent step near 150°C is most likely due to the loss of the coordinated water ligands (Figure 3.25). Elemental analysis predicted a similar percent solvent loss of 20.58%. All three bilayer graphs indicated that the framework of the red bilayer crystals began to decompose at approximately 225 °C and were completely decomposed after approximately 325°C (Figures 3.23-3.25).

The graphs for the 1D chain crystals show the same trends as the elemental analysis data for the loss of water and ethanol, but the 1D chain structure appears to be more stable, decomposing at approximately 275°C (Figures 3.26-3.28). The 1D chain crystals as synthesized (Figure 3.26) had an 18-20% mass loss which was comparable to the 20.97% loss calculated using elemental analysis. For the dried 1D chain crystals (Figure 3.27), only a 2-3% loss of mass was observed at lower temperatures. This could be due to the loss of small amounts of remaining ethanol or coordinated water. For the water-resolvated 1D chains, 17-19% mass was lost. This value was very similar to the 17.19% elemental analysis solvent percent value. Two steps are noticeable in the graph (Figure 3.25) suggesting that first water in the pores evaporated and then at higher temperatures, water coordinated to the cobalt atom was removed.

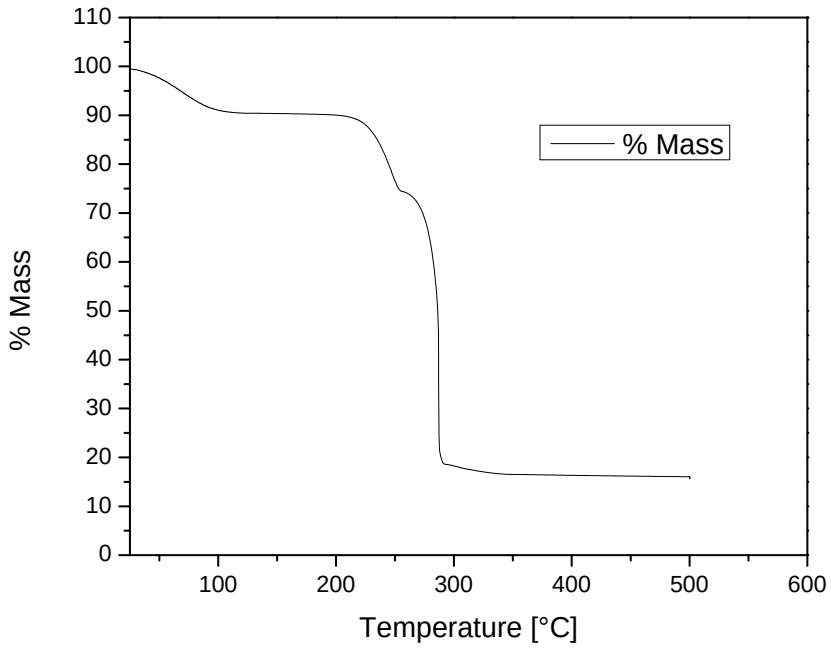

Figure 3.23 TGA data on red bilayer crystals in ethanol

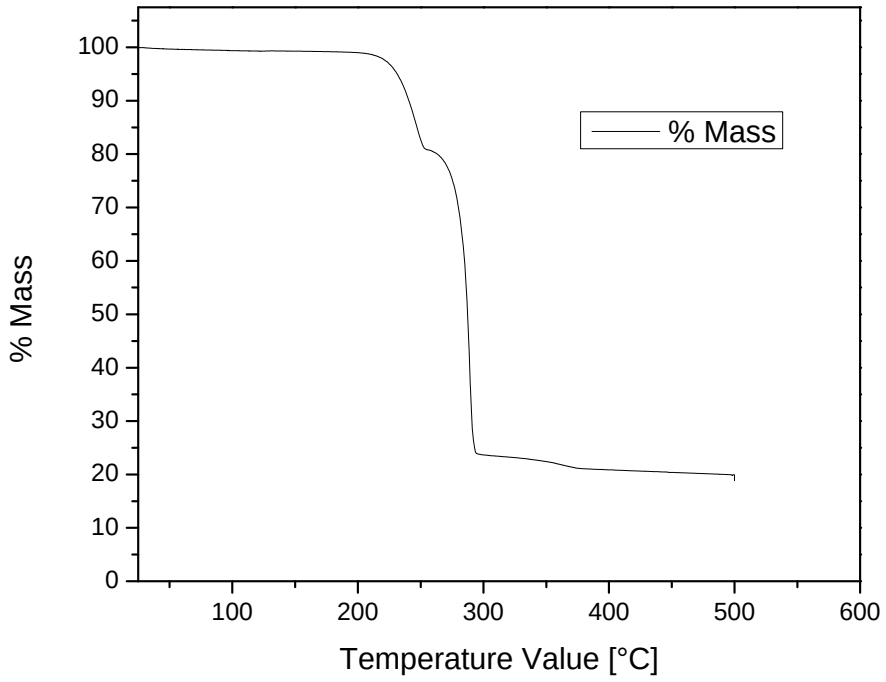

Figure 3.24 TGA of dried bilayer crystals

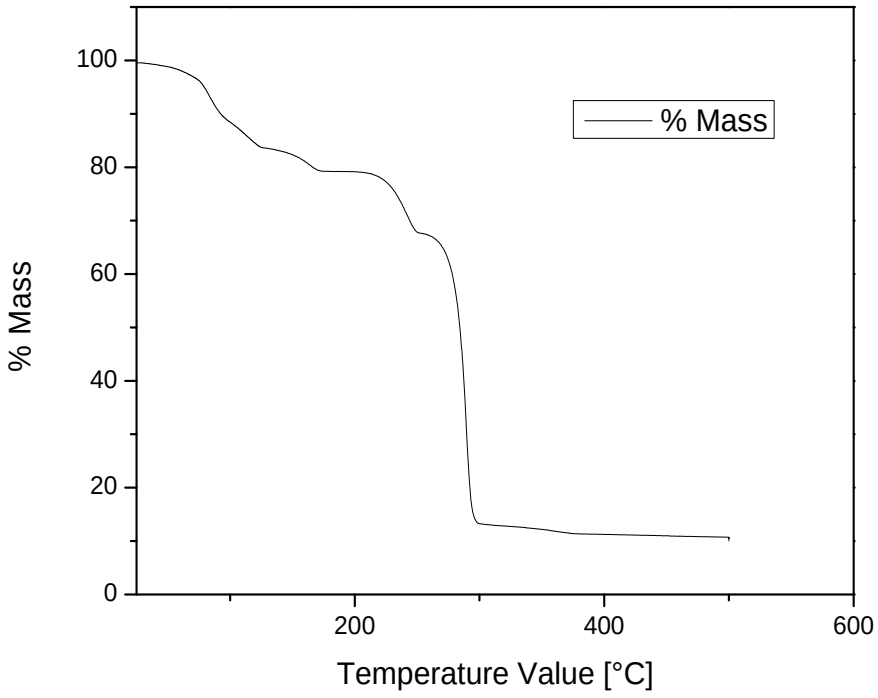

Figure 3.25 TGA data on water-resolvated dried bilayer crystals

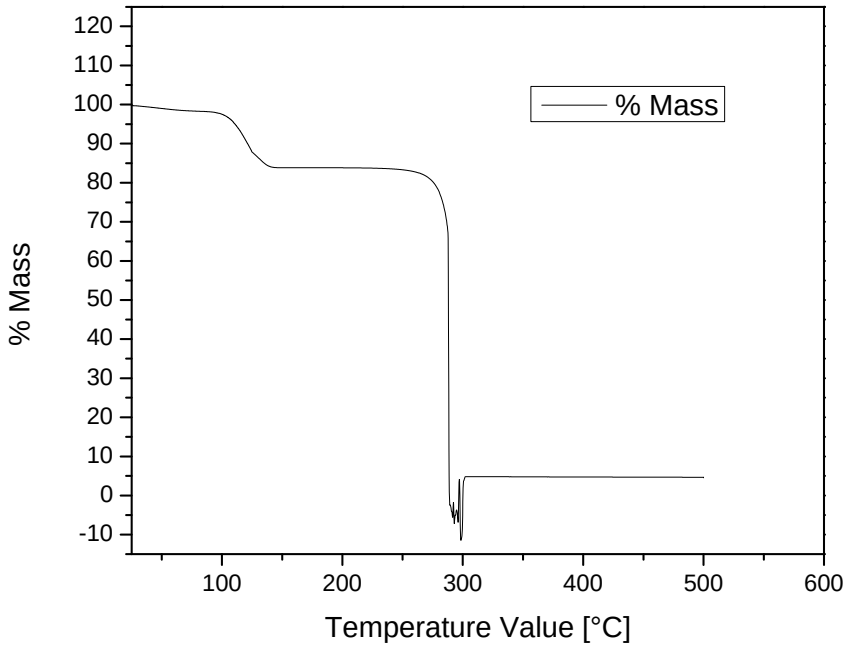

Figure 3.26 TGA data on 1D chain crystals as synthesized

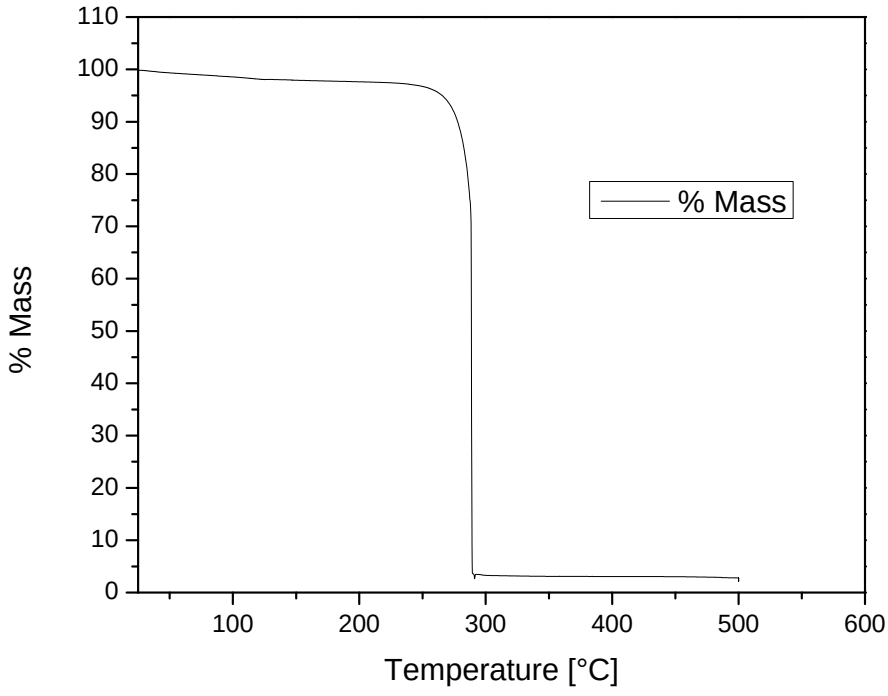

Figure 3.27 TGA data on dried 1D chain crystals

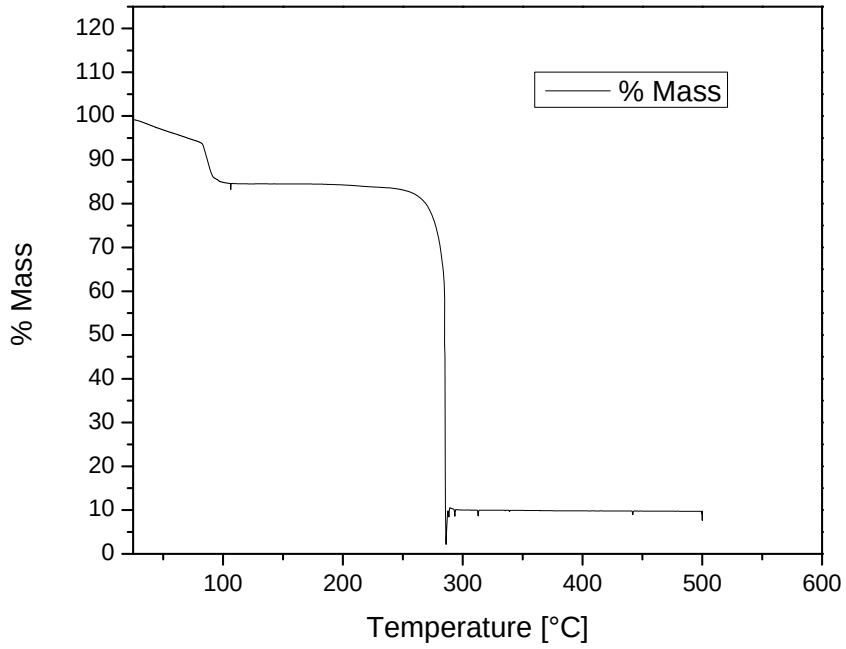

Figure 3.28 TGA data on dried 1D chain crystals exposed to water

Sorption Studies on Bilayer Using GC-MS

Two different methods of sorption studies were used to ascertain whether the red bilayer crystal pores showed a preference for particular organic solvents.

Method 1

Percent ethanol gas chromatography results for crystals synthesized in ethanol and added to a solution containing ethanol in 1-propanol did not show significant solvent exchange. This was most likely due to noise generated in the data from ethanol on the surface of the crystal (Figure 3.29). The small amount of solvent exchange also suggested that the pores took longer than 2 hours to complete the adsorption process.

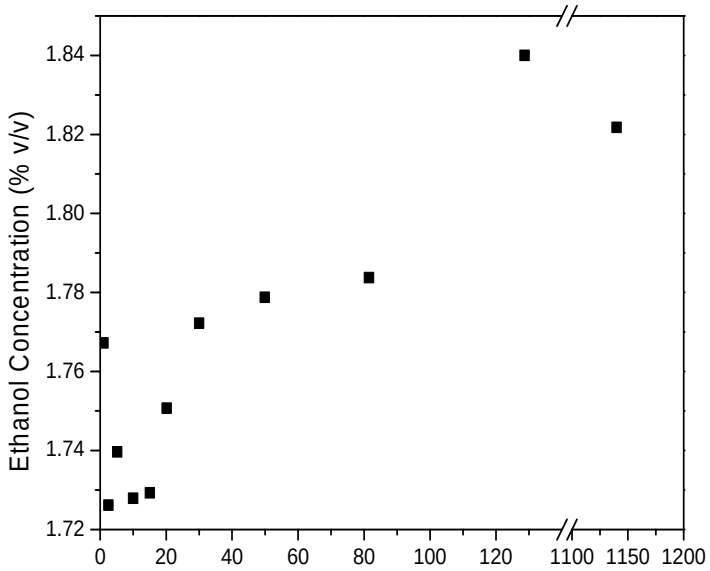

Figure 3.29 Concentration of ethanol desorption from the pores of the bilayer crystals into 1-propanol

Method 2

In only two of the studies of competitive sorption of two solvents into dried bilayer crystals showed a preference for a particular liquid guest molecule (Figures 3.30 and 3.31). Results indicated that at least a week was needed to observe significant changes in the solution compositions, as indicated by the peak area ratios. A preference was observed for ethanol over 1-pentanol. This is most likely due to the smaller size of the ethanol molecule (Figure 3.30). Also, the smaller molecule *n*-hexane was preferred over toluene in Figure 3.31. No preference is observed for toluene versus cyclohexane within

the pores and this is most likely due to their similar sizes (Figure 3.32). No preference was observed between ethanol and toluene in the bilayer pores as well (Figure 3.33). It is possible that ethanol and toluene interact equally with the framework. Ethanol participates in hydrogen bonding and toluene experiences π- π bonding with the framework.

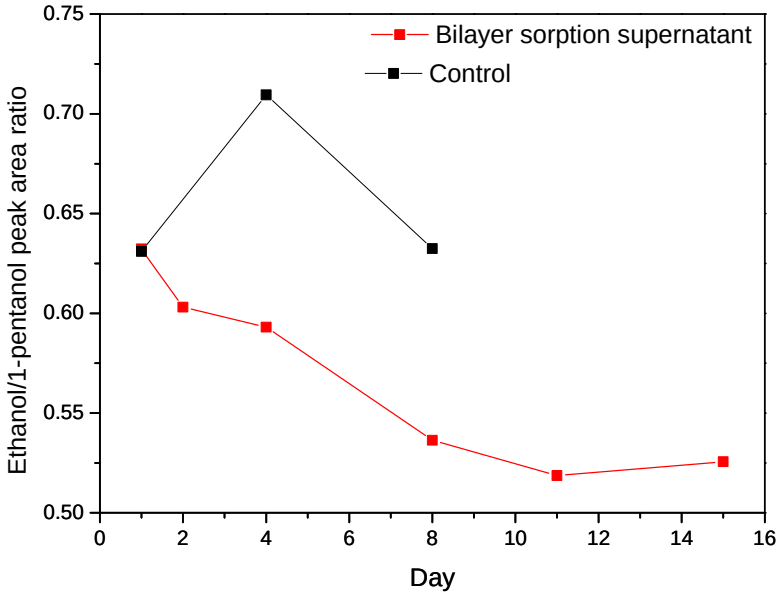

Figure 3.30 Equal parts mixture of ethanol and 1-pentanol using a crystal sample in solution and control

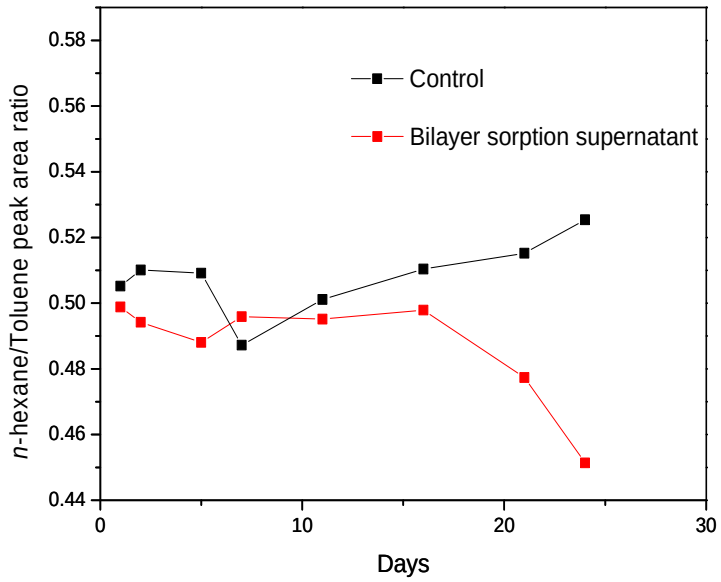

Figure 3.31 Peak area ratios collected using a crystal sample in binary solution and binary solution control of *n*-hexane and toluene.

The results of these sorption measurements are useful for determining the bilayer crystal pore selectivity. From the data, it is apparent that molecular size is one of the most important factors. Also, intermolecular interactions seem to be crucial as well as in the ethanol and toluene sample (Figure 3.33). The bonds formed between the guest molecule and the crystalline pore structure allows both large and small molecules that can interact with the framework to enter, resulting in no change in ratio.

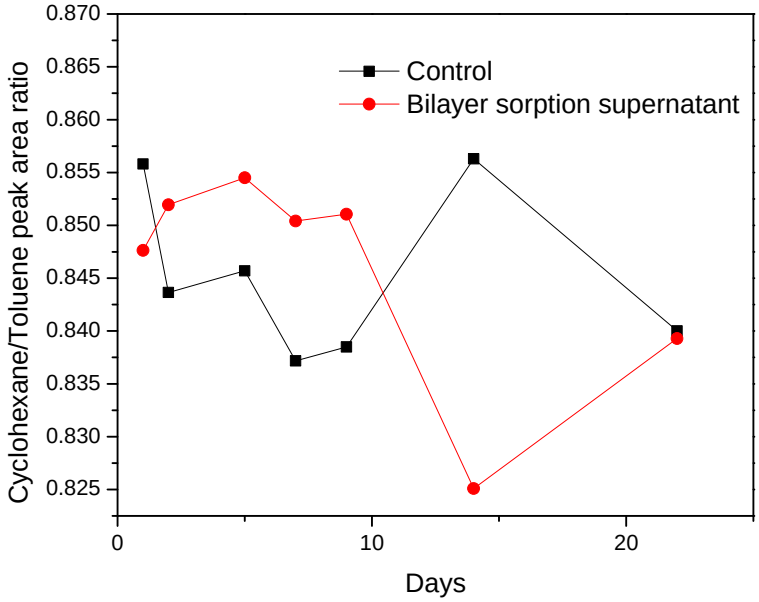

Figure 3.32 Cyclohexane/toluene

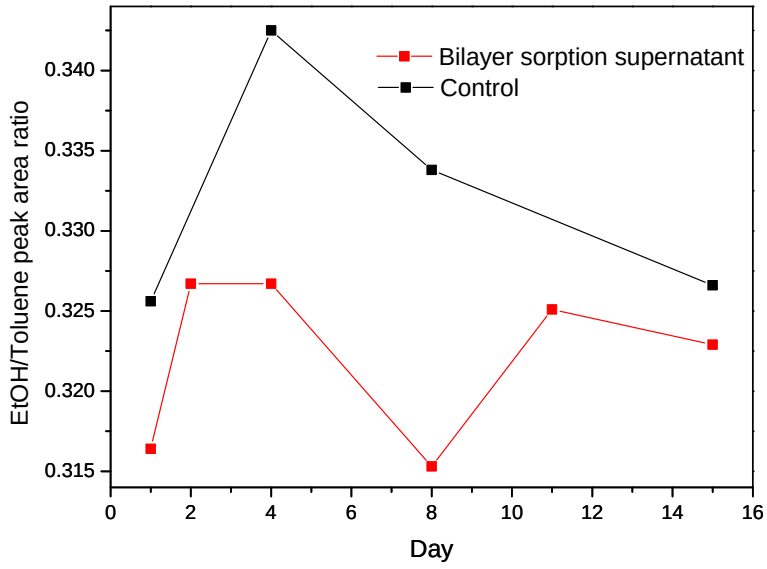

Figure 3.33 Equal parts mixture of ethanol and toluene

CHAPTER 4

CONCLUSIONS

Metal-organic frameworks made from cobalt nitrate and 4,4′-bipyridine have been shown to have many significant properties. While synthesizing the known, red bilayer crystals, a new, orange 1D chain crystalline framework was formed. The growth of this orange 1D framework was controlled by the addition of precise amounts of water. The red bilayer crystals could be produced in larger amounts compared to the 1D orange chain crystals as high concentrations of the components would often prevent 1D orange chain synthesis. Experimenting more with the concentrations of the metal and ligand components could result in finding a way to produce larger amounts of 1D orange chain crystalline product.

When the 1D orange chain crystals were dried, it was found that they still retained their single crystallinity and resulted in the formation of new, purple 1D chain crystals. Resolvation of water vapor into the purple 1D chain crystals restored the original structure, but resulted in a loss of single crystallinity. The dried red bilayer crystals could be resolvated with ethanol vapor, returning to their original, as synthesized structure. In the future it would be useful to test the bilayer stability over multiple desorption and resorption trials to see if it continuously maintains its crystallinity.

The presence of water seemed to affect not only the 1D chain structures, but also the red bilayer crystals. Slight amounts of water, even air humidity could bind to the cobalt atom and alter the bilayer crystal structure. The fact that water coordinated to the cobalt

metal for both the 2D and 1D framework but the organic solvent acetonitrile, a potential ligand ,did not shows that the frameworks are selective in the coordination of solvent to the Co.

TGA and elemental analysis data showed that the pores of these frameworks could hold large mass percentages of solvent. This suggested that the pores were capable of liquid guest exchange. Size was a prominent factor for the solvent molecule preference of the red bilayer pores. It would be useful to test the same solvents using the 1D chain crystals instead. The smaller pore structure could produce clearer solvent preference data, providing more understanding as to how the solvents interact with the crystals.

REFERENCES

1 Power, K. N.; Hennigar, T. L.; Zaworotko M.J. Crystal structure of the coordination polymer $[Co(bipy)_{1.3}(NO_3)_2]$ CS_2, a new motif for a network sustained by 'T-shape' building blocks. *New J. Chem.* **1998,** 177-181.

2 He, H.; Collins, D.; Zhao, X.; Zhang, G.; Ma, H.; Sun, D. Construction of metal-organic frameworks with 1D chain, 2D grid, and 3D porous framework based on a flexible imidazole ligand and rigid benzenedicarboxylates. *Crys. Gro. Des.* **2010**, *10*, 895-902.

3 Choi, H. J.; Lee, T.S.; Suh, M. P. Self-assembly of a molecular floral lace with one-dimensional channels and inclusion of glucose. *Angew, Chem. Int. Ed.* **1999**, *38*, 1405-1408.

4 Aijaz, A.; Barea, E.; Bharadwaj, P. K.; Diamondoid three-dimensional metal-organic framework showing structural transformation with guest molecules. *Crys. Gro. Des.* **2009**. *9*, 4480-4486.

5 Alaerts, L.; Maes, M.; Giebeler, L.; Jacobs, P. A.; Martens, J. A.; Denayer, J. F. M.; Kirschhock, C. E. A.; De Vos, D. E. Selective adsorption and separation of ortho-substituted alkylaromatics with the microporous aluminum terephthalate MIL-53. *J. Am. Chem. Soc.* **2008,** *130,* 14170-14178.

6 Yang, C.; Yan, X. Metal-organic framework MIL-101 (Cr) for high performance liquid chromatographic separation of substituted aromatics. *An. Chem.* **2011,** *83,* 7144-7150.

7 Gudbjarstson, H.; Biradha, K.; Poirier, K. M.; Zaworotko, M. J. Novel nanoporous coordination polymer sustained by self-assembly of T-shaped moieties. *J. Am. Chem. Soc*. **1999,** *121,* 2599-2600.

8 Han, S.; Wei, Y.; Valente, C.; Lagzi, I.; Gassensmith, J. J.; Coskun, A.; Stoddart, J. F.; Grzybowski, B. A. Chromatography in a single metal-organic framework MOF crystal. *J. Am. Chem. Soc.* **2010,** *132,* 16358-16361.

9 Chen, B.; Wang, L.; Zapata, F.; Quian, G.; Lobkovsky, E. B. A luminescent microporous metal-organic framework for the recognition and sensing of anions. *J. Am. Chem. Soc*. **2008,** *130,* 6718-6719.

10 Fletcher, A.J; Cussen, E. J.; Piror, T. J.; Rosseinsky, M. J.; Kepert, C. J.; Thomas, K. M. Adsorption dynamics of gases and vapors on the nanoporous metal organic framework material Ni_2(4,4'-bipyridine)$_3$(NO_3)$_4$: guest modification of host sorption behavior. *J. Am. Chem. Soc.* **2001,** *41,* 10001-10011.

11 Jiang, H. Porous metal-organic frameworks as platforms for functional applications. *Chem. Commun.* **2011,** *47,* 3341-3370.

12 Nelson, A. P.; Parrish, D. A.; Cambrea, L. R.; Baldwin, L. C.; Trivedi, N. J.; Mulfort, K. L.; Farha, O. K.; Hupp, J. T. Crystal to crystal guest exchange in a mixed ligand metal-organic framework. *Crys. Gro. Des.* **2009,** *9,* 4588-4591.

13 Smith, M.; Culp, J. T.; Bittner, E.; Parker, B.; Li, J.; Bockrath, B. Kinetics of desorption of hexane from the microporous metal organic framework RPM-1. *Micr. Meso. Mat.***2007,** *106,* 115-121.

14 Wang, S.; Ma, J.; Li, L.; Chen, T.; Sun, Z.; Luo, J. Guest exchange dynamics in a flexible bilayer porous coordination polymer. *Inorg. Chem Commun.* **2012,** *16*, 65-69.

15 Gu, Z.; Pang, C.; Lia, Z.; Xia, H. A cobalt(II) metal–organic framework with all-cis 1,2,3,4,5,6-cyclohexanehexacarboxylate ligand: Synthesis, structure, and magnetic properties *Inorg. Chem. Commun.* **2012**, *24*, 237-240.

16 Hadler, G. J.; Kepert, C. J.; Moubaraki, B.; Murray, K.S.; Cashion, J. D. Guest dependent spin crossover in a nanoporous molecular framework material. *Sci.* **2002,** *298*, 1762-1765

17 Allendorf, M. D.; Bauer, C. A.; Bhakta, R. K.; Houk, R. J. T. Luminescent metal-organic frameworks. *Chem. Soc. Rev*. **2009,** *38,* 1330-1352.

18 Biswas, S.; Maes, M.; Dhakshinamoorthy, A.; Feyand, M.; De Vos, D. E.; Garcia, H.; Stock, N. Fuel purification, lewis acid and aerobic oxidation catalysis performed by a microporous Co-BTT (BTT3- = 1,3,5-benzenetristetrazolate) framework having coordinatively unsaturated sites. *J. Mater. Chem.* **2012,** *22,* 10200-10209.

19 Qiu, Ling-Guang; Gu, Li-Na; Hu, Gang; Zhang, Li-De. Synthesis, structural characterization and selectively catalytic properties of metal-organic frameworks with nano-sized channels: A modular design strategy. *J. Sol. S. Chem.*. **2009**, *182*, 502-508.

20 Gomez-Lor, B.; Gutierrez-Puebla, M.; Iglesias, M.; Monge, M.A.; Ruiz-Valero, C.; Snejko, N. $In_2(OH)_3(BDC)_{1.5}$ (BDC=1,4-benzendicarboxylate): An In(III) supramolecular 3D framework with catalytic activity. *Inorg. Chem.* **2002,** *41*, 2429-2432.

21 Henschel, A.; Senkovska, I.; Kaskel, S. Liquid-phase adsorption on metal-organic frameworks. *Adsorp.* **2011,** *17*, 219-226.

22 Sheldrick, G. M. A short history of SHELX. Acta Cryst. **2008**, *64*, 112-122

23 Howard A. K.; Puschmann, H. OLEX2 a complete structure solution, refinement and analysis program. *J. Appl. Cryst.* **2009**. *42*, 339-341